ΠΑΝΕΠΙΣΤΗΜΙΟ ΚΡΗΤΗΣ
UNIVERSITY OF CRETE

2D Hybrid Double Halide Perovskites and Layered Perovskites based on Lead

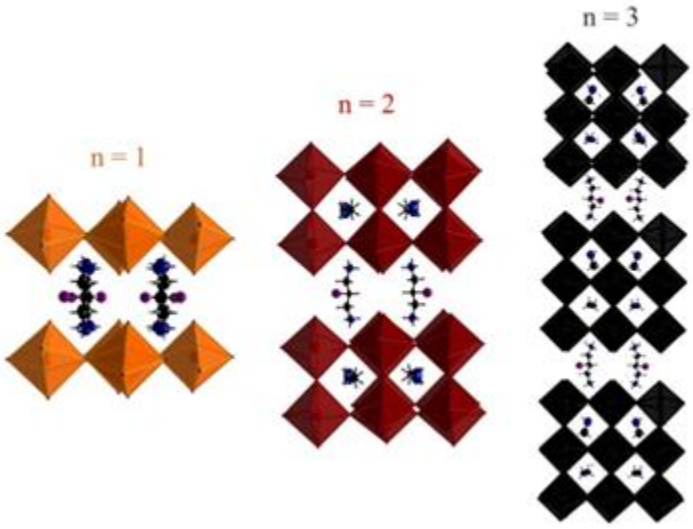

Maria Maniadi

Crystal Chemistry Lab
Constantinos C. Stoumpos Ph.D.

Inorganic Chemistry Lab
Nicolas Mercier Ph.D.

University of Crete
Department of Materials Science and Technology

ACKNOWLEDGEMENT

I would like to thank my supervisors Costantinos C. Stoumpos from the University of Crete who helped me evolve my skills and knowledge on the perovskite field. A field I grew to love and have the curiosity to further explore.

Moreover, I would like to thank my second supervisor, Nicolas Mercier from the Université d'Angers, who gave me the opportunity to work with him at his laboratory. Also, I would like to thank my colleagues from the Université d'Angers who helped on the second part of this thesis and thank my coworkers from the Crystal Chemistry Lab, too.

TABLE OF CONTENTS

ABSTRACT

2D halide perovskite semiconductors have shown a variety of applications in recent years, mainly in photovoltaics, attracting a plethora of scientists to this developing multidisciplinary field. The primary goal for this Thesis, is to further exploring the field, by synthesizing new 2D hybrid halide perovskites and trying to optimize certain aspects of the crystal and electronic band structure. Towards this end, the new organic diammonium spacer (2-halo, 1,3-diammino propane, DicX, X = Br, I) was introduced, in an attempt to examine the effect of the organic halide in the photophysical properties of the layered perovskites. The new spacer was employed towards the synthesis of the 2D homologous series (DicI)$(CH_3NH_3)_{n-1}Pb_nI_{3n+1}$ (n = 1-3) as well as the synthesis of members of the corresponding 2D lead-free compounds based on ordered double perovskites combining Ag+ and Bi3+ double perovskites.

As it was shown from optical measurements in the visible range, new compounds exhibit stable excitons at room temperature emitting in the wavelength range λ = 500-650nm consistent with their Multiple Quantum Well electronic structure. However, unlike other derivatives of the 2D perovskites, the binding energy of the materials appears to be significantly reduced, as a result of the organic spacer. The extra organ iodide in the spacer reduces the dielectric contrast between the organic and the inorganic components whereas the interlayer distance between the perovskite sheets is significantly reduced from the short carbon chain. As band structure calculations also support, the new materials effectively behave as bulk perovskites, resulting in a charge-transport in all three dimensions, a property that may have great impact in the application of these materials in solar cells. In an attempt to take advantage of this property, thin films of these layered 2D halide perovskites were fabricated and characterized. Future work on these materials will deal with the manufacture and characterization of full solar cells devices, where it is anticipated that we will be able to obtain a significant increase in the photo-generated current which may lead to an overall improved power-conversion efficiency.

INTRODUCTION

A brief history about perovskites

Perovskites is an extensive class of solid with a general formula ABX_3 combining a wide variety of metallic elements with certain nonmetals, usually oxygen, possessing a crystal structure-specific atomic arrangement. Due to perovskite's diversity and variety, they can form insulators, semiconductors, superionic conductors (whole ions, not just electrons, flowing through the crystal), as well as metal-like conductors[1]. The term ''perovskite'' was first introduced from a Russian scientist, Gustav Rose in 1839, in order to describe the mineral comprising of calcium titanium and oxygen ($CaTiO_3$). This mineral was named after its discoverer, the Russian mineralogist Lev Alekseyevich von Perovski[2, 3]. Approximately a century later, in 1926 Victor Goldschmidt[2] was the first to use the term "perovskite" in a general sense in order to classify the compounds with ABX_3 chemical composition and the specific atom arrangement to define a unique crystal structure group. Despite being the dominant fraction of the perovskite family, oxides are not the only compounds that can form the perovskite structure.

Halide perovskites, where a halogen occupies the position of the X-site, have also been known for a long time, yet, due to the different physical of the solids (oxides vs halides) the two subclasses have been evolved nearly independently. Thus, the first alkali-metal lead halide perovskites were synthesized in 1893[4], but their crystallographic structures and photoconductive properties were only determined in the 1950's[5] by Christian Møller. Meanwhile, Pb-free perovskites were also developed independently, most notably through the efforts of Auger and Karantassis, who prepared new families of perovskites in the form of $CsSnX_3$[6] (1925) and $CsGeX_3$[7] (1935). The first hybrid inorganic-organic perovskite, was demonstrated in the work of Dieter Weber's, who discovered $CH_3NH_3SnX_3$ and $CH_3NH_3PbX_3$, in 1978[8]. In 2009, the field of halide perovskites "exploded", owing to the work of Tsutomu Miysaka[9], who demonstrated for the first time that $CH_3NH_3PbI_3$ can be used for practical applications, specifically, in the construction of efficient solar cells using the halide perovskite semiconductors as the light absorber. Since then, halide perovskites have evolved to an emerging class of semiconductors with unique physicochemical properties.

Layered perovskites, started to introduce themselves in the field of perovskites in the form of oxides during 1950s, where S.N. Ruddlesden and O. Popper described the structures of Sr_2TiO_4 and $Sr_3Ti_2O_7$[10-13]. The latter was determined to be a mixture of two perovskite layers. During this time, they could only prove the existence of n=1 and n=2 and could only assume the possibility of synthesizing more layers, at least n=3 and n=4. In 1960s, the

ferroelectric properties of these compounds became well known attracting more researchers on the field[14]. Another material which looks a lot like the oxide perovskites S.N. Ruddlesden and O. Popper described, is the $YBa_2Cu_3O_{7-x}$ (YBCO)[15]. These materials proved to be superconductors after oxidation occurs and have found applications in the fabrication of thin films[15-17]. The last decade, layered halide perovskites became popular as they have great potential for creating great efficiency solar cells[18-20]. The monolayer and the multilayered counterparts of these compounds exhibit exitonic properties as well as quantum and dielectric confinement effects, making them ideal for studying quantum wells physics at ambient temperature. Ruddlesden and Popper's hypothesis was proved valid for halide perovskites as well, as many perovskite with more than n=4 layers[19, 21, 22] have been reported with the record being n=7[8, 23].

The Halide Perovskite Structure

The general chemical formula ABX_3 describes the general crystal structure of a halide perovskite. A is a monovalent cation, usually Cs^+, $CH_3NH_3^+$ $(MA)^+$ or $HC(NH_2)^{2+}$ $(FA)^{2+}$ as these three are the only ones able to stabilize the perovskite structure to date. B is a divalent metal cations which can be selected by a limited set of elements including alkaline earths, the bivalent rare earths and the heavier group 14 elements (Ge^{2+}, Sn^{2+}, Pb^{2+}) and X is a halide anions (Cl^-, Br^- or I^-)[24, 25]. The B cations are coordinated with X anions forming $[BX_{6/2}]^{4-}$ octahedra that share corners in all three orthogonal directions, forming cuboctahedra voids. The center of the octahedron is occupied by the B cations with the X anions occupying the six apices of the octahedron, while the A cations fill the voids generated between the corner-connected octahedra.

2D Halide Perovskites

The perovskite structure is significant not only in its pristine form but also because it can form several perovskite-like derivatives. One family of these derivative perovskites is hybrid organic-inorganic perovskites that have been demonstrated in diverse optoelectronic applications[26, 27]. Early exploration of these 2D perovskites for optoelectronic application was mainly conducted by Mitzi, Tsutsui, and their coworkers. In the 1980s, Ishihara et al were the first to manufacture lead-based organic-inorganic hybrid halide perovskites with n=1[28]. Also, the first halide organic-inorganic perovskite (HOIP) was synthesized by Dieter Weber in 1978[29]. It was described with the chemical compound of methyl ammonium lead iodide ($MAPbI_3$), which properties were tested in the early 1990s by Mitzi and coworkers[30]. Moreover, another essential work was reported, in 1999 by Mitzi and coworkers, on thin film field-effect transistor using p-type $(C_6H_5C_2H_4NH_3)_2SnI_4$. Furthermore, the usage of organic-

inorganic hybrid perovskites (e.g., $CH_3NH_3PbBr_3$ and $CH_3NH_3PbI_3$) as light sensitizers were reported in 2009 by Kojima and coworkers and was the seminal work that initiated the halide perovskite era [31].

The other main family of these derivatives structures is that of the two-dimensional (2D) perovskites. Although, research on 2D halide perovskites had been conducted since the mid-60s, Maruyama et al.[32] were the first to report the new layered material, in 1986, which held the formula compound of $(CnH_{(2n+1)}\ NH_3)_2MX_4$[28], where M^{2+} = Ge^{2+}, Sn^{2+}, Pb^{2+}. The properties of these, new at the time, materials were studied by Thorn, Ishihara, and Papavassiliou in the 1990s [8, 33]. Based on the ability of halide perovskites to create homologous series, Thorn and coworkers proposed the hypothesis of "in between faces". This hypothesis introduced the main conceptual relationship between the standard 2D oxide perovskites and the 2D hybrid halide perovskites. Moreover, Ishihara and coworkers, described the 2D with lead iodide perovskites as multiple quantum wells with semiconducting inorganic wells separated by insulating organic barriers[30]. Later on, Mitzi and his colleagues fabricated single layer (n=1) 2D halide perovskites, using a variety of larger metal ions, such as Ge^{2+}, Sn^{2+} and bivalent rare earth elements.

2D halide perovskites form by slicing the 3D crystal structure across specific crystallographic directions. When the cleavage occurs across the (100) plane of the ideal cubic perovskite there are two major types of 2D perovskites that can arise, Ruddlesden–Popper (RP) and Dion–Jacobson (DJ)[31].The latter hasn't been investigated a lot, as it is a relatively rare type for halide perovskites. In contrast, the former family has been extensively studied in recent years. The general chemical formula of RP perovskites is $(RNH_3)_2A_{n-1}B_nX_{3n+1}$. The R in the formula represents organic moieties attached to the $-NH^{3+}$ cationic group, with the most extensively studied cation being phenethyl ammonium (PEA) or butyl ammonium (BA)[2, 34-36]. In 2D perovskites, A-sites are also occupied by a monovalent cation such as Cs^+, MA^+ or FA^+, while B-sites are also limited to the metals available for the 3D perovskite. An additional feature of the 2D perovskites is the thickness of the perovskite sheet, which is denoted by the n variable (n is an integer), in the chemical formula, indicating the number of metal halide monolayers between the two $(RNH_3)_2$ layers. As mentioned above, each layer is composed of metal halide octahedra, which are sandwiched between bilayer of bulky organic cations and certainly could exist along different crystal directions.

2D halide perovskites have many applications due to their unique properties. Compared to the 3D metal halide perovskites, layered 2D perovskites are a promising candidate for flexible electronic and potential photonic applications, as they can be fabricated on a diversity of substrates including plastics owing to the low-temperature solution processing. Furthermore,

due to their high light absorption coefficient, fast carrier transport and low-temperature solution process ability, these materials found applications on solid Dye-Sensitized Solar Cells (DSSCs) by replacing both the ruthenium sensitizer and the electrolyte[24, 33, 37]. Moreover, these materials are used in photo detectors and LED materials, due to the fact that they are highly sensitive to the visible light and exhibit intriguing optical and electrical properties.

2D Double Halide Perovskites

Recent years have seen the emergence of more complex compositions in the form of 2D double halide perovskites[27, 38-42], driven by the need to replace Pb with less toxic metals while maintaining the magnificent properties of the heavy metal perovskites. The general chemical formula of double halide perovskites, is $A'A_{n-1}(M(I)_{0.5}M(III)_{0,5})_nX_{3n+1}$. It derives from the ideal 2D structure A_2BX_4. By replacing the divalent metal with a pair of metals with an average charge of +2. The most common variations have seen the combination of monovalent cations such as Ag^+, Au^+ and Tl^+, and a trivalent cation, such as Fe^{3+}, Au^{3+} and Bi^{3+}. The additional metals offer a large degree of complexity which allows the research towards new and unconventional material with a great potential to reveal unusual physical properties.

Layered Halide Perovskites

The last decade, layered halide perovskites became popular as they have great potential for creating great efficiency solar cells[18-20]. The monolayer and the multilayered counterparts of these compounds exhibit exitonic properties as well as quantum and dielectric confinement effects, making them ideal for studying quantum wells. The general chemical formula of layered halide perovskites, is $(A')_{2(}A)_{n-1}M^{II}{}_nX_{3n+1}$, (where A' is a suitable spacer cation), A is the perovkitizer (that filles the empty spaces between the octahedra) and the n variable (n is an integer), denotes the number (thickness) of these metal halide monolayers between the organic spacer layers[30, 38, 39, 42, 43]. The M is a metal with oxidation state of 2+, Pb is most commonly used.

In this Diploma Thesis, we are investigating two different aspects of layered halide perovskites in two related but distinctively different projects.

The first part of this diploma thesis, concerns the synthesis of 2D double perovskites combining two metals (M^+ = Ag, M^{+3} = Bi, Sb, X = Br) in a solution of HBr acid and the resulting 1D group-15 metal perovskites when the same experiments conducted in HI acid (X = I). The new compounds were characterized and the crystal structures were determined via single-crystal X-ray diffraction, whereas the optical properties of the materials reveal that they exhibit weak emission. The two new 2D double perovskite compounds are promising

candidates in replacing Pb-based perovskites in wide bandgap applications, such as radiation detection and solid-state lighting.

The second part concerns the synthesis of a new n series with general stoichiometry of $(A)(MA)_{n-1}Pb_nI_{3n+1}$, where A is the 2-iodopropane-1,3-diamonium dibromide dication [(DicI)2+ 2I-] and MA is the methylammonium cation Pure phases of n= 1-3 (X = I) crystals have been obtained fully characterized, including the crystal structure determination via single-crystal X-ray diffraction. These Dion Jacobson-type compounds are unique due to extra iodine ion of the organic molecule, creating short I-I bond distances between the layers that infer drastic changes in the electronic structure of these materials. Thin-films of these perovskites were also obtained via the spin coating process, towards applications in photovoltaic cells.

METHODS

A. General Information

PbI_2 (99.9%), PbO (99.9%), hydroiodic acid (57 wt % in H2O, distilled, stabilized, 99.95%), and hypo phosphorous acid solution (50 wt % in H2O), hydro bromic acid (HBr, 48% w/w in H_2O), silver bromide (AgBr, 99%), silver iodide (AgI, 99%), bismuth (III) bromide ($BiBr_3$, 99%), bismuth (III) iodide (BiI_3, 99%), antimony (III) bromide ($SbBr_3$, 99%) and MAI (>99.5%) were purchased from Sigma-Aldrich and used as received. MABr (90.5%), $(DicBr)^{2+}$ $2Br^-$ (85.5%) and $(DicI)^{2+}$ $2I^-$ (85.5%) were synthesized in the Crystal Chemistry Laboratory of Université d'Angers.

Synthesis

I. Synthesis of the Dication with Iodide and Bromide

2,2,12,12-tetramethyl-4,10-dioxo-3,11-dioxa-5,9-diazatridecan-7-yl methane sulfonate compound had been obtained previously in the lab according to the reaction as described by Ramalingam et al[44].

2-iodopropane-1,3-diamonium diiodide [$(DicI)^{2+}$ $2I^-$]: 1gr of 2,2,12,12-tetramethyl-4,10-dioxo-3,11-dioxa-5,9-diazatridecan-7-yl methane sulfonate was introduced into a 10mL flask and HI acid was added dropwise till the liquid covered the whole amount of the solid (~2mL) . The solution was left to stir overnight at 75℃ under reflux. The system was plugged by a septum with a needle stuck in it to make the isobar. The next day, stirring was discontinued and ethylene acetate was added into the reaction and left there for 2hours for the salt of $(DicI)^{2+}$ $2I^-$ fully precipitate. The precipitated compound was filtered and washed with ethylene acetate. The salt was placed in the oven to dry at 70℃ for 1hour. Yield: 85.5%. Nuclear Magnetic Resonance

spectroscopy was used in order to identify the compound along with SCXRD and XRD measurements as shown in the **Scheme 1** of the **Appendix**.

2-bromopropane-1,3-diamonium dibromide [$(DicBr)^{2+}$ $2Br^-$]: 1gr of 2,2,12,12-tetramethyl-4,10-dioxo-3,11-dioxa-5,9-diazatridecan-7-yl methane sulfonate was introduced into a 10mL flask and HBr acid was added dropwise till the liquid covered the whole amount of the solid (~2mL). The solution left to stir over night at 75℃ under reflux. The system was plugged by a septum with a needle stuck in it to make the isobar. The next day, stirring was discontinued and ethylene acetate was added into the reaction and left there for 2hours for the salt of $(DicBr)^{2+}$ $2Br^-$ fully precipitate. The precipitated compound was filtered and washed with ethylene acetate. The salt was placed in the oven to dry at 70℃ for 1hour. Yield: 85.5%.

II. 2D Double Halide Perovskites

$(DicBr)_2AgBiBr_8$: HBr (3mL) was added to a mixture of $AgNO_3$ (38.5mg, 1mmol), $BiBr_3$ (178.1mg, 1mmol) and $(DicBr)^{2+}$ $2Br^-$ (139.6mg, 2mmol) in a 20mL scintillation vial. The resulting mixture was magnetically stirred and was heated under stirring to 150℃. After 30 minutes, the reaction was allowed to cool to ambient temperature. After 1-day, yellow plate-like crystals precipitated at the bottom of the vial. The resultant precipitate was isolated via suction filtration and washed with acetone. Yield: 573.8mg (52.4%)

$(DicBr)_2AgSbBr_8$: HBr (3mL) was added to a mixture of $AgNO_3$ (38.5mg, 1mmol), $SbBr_3$ (178.1mg, 1mmol) and $(DicBr)^{2+}$ $2Br^-$ (139.6mg, 2mmol) in a 20mL scintillation vial. The resulting mixture was magnetically stirred and was heated under stirring to 150℃. After 30 minutes, the reaction was allowed to cool to ambient temperature. After 1-day, yellow plate-like crystals precipitated at the bottom of the vial. The resultant precipitate was isolated via suction filtration and washed with acetone. Yield: 585.4mg (53.7%)

III. 1D Halide Perovskites

$(DicI)_2BiI_5$: HI (4mL) and H_3PO_2 (0.5ml) were added to a mixture of BiI_3 (59.0mg, 0.1mmol), AgI (91.2mg, 0.1mmol) and $(DicI)^{2+}$ $2I^-$ (91.2mg, 0.2mmol) in a 20mL scintillation vial. The resulting mixture was magnetically stirred to 130℃, resulting in a clear red solution. After 30 minutes, stirring was discontinued and the reaction was allowed to cool naturally to ambient temperature. After 1day, dark purple crystalline powder precipitated at the bottom of the vial. The resultant precipitate was isolated via suction filtration and washed with ethylene acetate. Yield: 578.9mg (54.3%)

$(DicI)_2SbI_5$: HI (4mL) and H_3PO_2 (0.5ml) were added to a mixture of SbI_3 (50.3mg, 0.1mmol), AgI (91.2mg, 0.1mmol) and $(DicI)^{2+}$ $2I^-$ (91.2mg, 0.2mmol) in a 20mL scintillation vial. The

resulting mixture was magnetically stirred to 130℃, resulting in a clear red solution. After 30 minutes, stirring was discontinued and the reaction was allowed to cool naturally to ambient temperature. After 1hour, purple crystalline powder precipitated at the bottom of the vial. The resultant precipitate was isolated via suction filtration and cleaned with ethylene acetate. Yield: 577.6mg (54.0%)

IV. The Layered Compounds with Lead, $(Dic)(MA)_{n-2}Pb_nI_{3n+1}$

$(DicI)PbI_4 \cdot 1H_2O$ (n=1): HI (3mL) and was added to a mixture of PbI_2 (50.0mg, 0.1mmol) and $(DicI)^{2+}$ $2I^-$ (50.0mg, 0.1mmol) in a 20mL scintillation vial. The resulting mixture was magnetically stirred to 130℃, resulting in a clear yellow solution. After 30 minutes, stirring was discontinued and the reaction was allowed to cool naturally to ambient temperature. After 1day, yellow needle-shaped crystals precipitated at the bottom of the vial. The resultant precipitate was isolated via suction filtration and washed with ethylene acetate. Yield: 46.8mg (51.09%)

$(DicI)(MA)Pb_2I_7$ (n=2): HI (5mL) and H_3PO_2 (0.5ml) were added in a 20mL scintillation vial of PbO (334.5mg, 1.5mmol). After 5 minutes of stirring to 130℃, MAI (159.0mg, 1mmol) was added into the dissolved solution, resulting in a clear yellow solution. In another 20mL scintillation vial $(DicI)^{2+}$ $2I^-$ (114.0mg, 0.25mmol) are dissolved in HI (0.5ml) under heating and stirring to 200℃. After, the vial with the (DicI) becomes a clear solution we add its content into the first vial without any significant change in the color of the solution. The resulting mixture was magnetically stirred resulting in a clear yellow solution. After 30 minutes, stirring was discontinued and the reaction was allowed to cool naturally to ambient temperature. After 1day, red square-shaped crystals precipitated at the bottom of the vial. The resultant precipitate was isolated via suction filtration. Yield: 135.8mg (35.35%)

$(DicI)(MA)_2Pb_3I_{10}$ (n=3): HI (4mL) and H_3PO_2 (0.5ml) were added in a 20mL scintillation vial of PbO (446.0mg, 2mmol). After 5 minutes of stirring to 130℃, MAI (318.0mg, 2mmol) was added into the dissolved solution, resulting in a clear yellow solution. In another 20mL scintillation vial $(DicI)^{2+}$ $2I^-$ (45.6mg, 0.1mmol) are dissolved in HI (0.5ml) under heating and stirring to 200℃. After, the vial with the (DicI) becomes a clear solution we add its content into the first vial without any significant change in the color of the solution. The resulting mixture was magnetically stirred resulting in a clear yellow solution. After 30 minutes, stirring was discontinued and the reaction was allowed to cool naturally to ambient temperature. After 1day, black square-shaped crystals precipitated at the bottom of the vial. The resultant precipitate was isolated via suction filtration. Yield: 107.5mg (49.8%)

B. Characterization

Nuclear magnetic resonance (NMR): Nuclear Magnetic Resonance is an organic chemistry analysis technique to know and identify the molecule and its purity. A superconducting magnet, cooled by liquid helium, which is itself cooled by liquid nitrogen, of varying power, is used. It is comprised of a 300 MHz spectrometer. At the end of the analysis, a spectrum of intensity versus chemical shift in parts per million (ppm) is obtained. To obtain an answer after subjecting the sample to the magnetic field $\overrightarrow{B_0}$. Under the effect of this magnetic field, a degenerative lift-off is created under the Zeeman effect. The detection is done by the transition induced by $\overrightarrow{B_1}$. Atoms with an odd spin multiplicity 2I+1 are required, such as ^{1}H or the more commonly analyzed ^{13}C. A few milligrams of the product to be analyzed, solid or liquid, are introduced into a glass tube with approximately 1 mL of deuterated solvent as it serves as a reference. At the end of the measurement, the data is retrieved and processed via the MestRenova software.

Powder X-ray Diffraction (XRD): A Bruker D8 ADVANCE or a Rigaku SmartLab were (Cu Kα, λ = 1.5406 Å) used to analyze the powder patterns of the synthesized compounds and thin films. The samples were mounted in the Bragg-Brentano geometry (reflection mode) in θ-2θ measurements, allowing us to obtain a diffractogram of I=f(2θ) in the range of 2θ = 5 60°. The data collected and analyzed using EVA or SmartLab Studio II software, respectively.

Single Crystal X-ray Diffraction: Full-sphere data were collected using a Bruker D8 VENTURE diffractometer equipped with a Kappa goniometer stage, a PHOTON II CPAD detector, and an IμS 3.0 Mo Kα source (λ = 0.71073 Å). Data were collected at 293 K. The collected data were integrated and applied with multiscan absorption correction using the APEX3 software. Crystal structures were solved by charge flipping and refined (full-matrix least-squares on F^2) using the Jana2006 package[23].

Thermogravimetric analysis (TGA): A full set of data were adopted via Diamond TGA set up, which was purchased from Perkin Elmer Company. The TGA device consists of an electronic high accuracy weight scale, which is connected with a high temperature oven surrounding the supplement area. Data were measured in the 25-xxx ℃ under a continuous N_2 flow at a flow rate of 200 mL/min.

Differential Scanning Calorimetry (DSC): A full set of data were collected via DSC-250 for all n compounds. Approximately 2.3 mg of each sample were placed in aluminum pans which were then hermetically closed. They were placed in the calorimeter along with an empty reference pan. The samples were first maintained in a 2 min isothermal state and then heated from 30 ℃ up to 170 ℃ with a rate of 10 $℃/min$. The samples then maintained in a 2 min

isothermal state and then cooled from 170 ℃ down to 30 ℃ with a rate of 10 ℃/min. The process was repeated twice, with the first cycle discarded as it was performed only to erase the samples thermal history.

Optical Absorption Spectroscopy: Optical diffuse reflectance measurements were performed using a Shimadzu UV-2600 plus UV-vis-NIR spectrometer operating in the 185-1400 nm region using $BaSO_4$ as the reference of 100% reflectance. The band gap of the material was estimated by converting reflectance to absorption according to the Kubelka-Munk equation: $\frac{\alpha}{s} = \frac{(1-R)2}{2R}$, where R is the reflectance and α and S are the absorption and scattering coefficients[45], respectively.

Photoluminescence Spectroscopy (PL): Photoluminescence spectra were collected on oriented crystals of the (Dic)$(MA)_{n-1}Pb_nI_{3n+1}$ perovskites (n = 2 and 3) using Horiba LabRam Evolution high resolution confocal Raman microscope spectrometer (600 g/mm diffraction grating) equipped with a diode CW laser (532 nm, 35 mW) and a Synapse CCD camera. The incident laser beam was parallel to the (010) direction of the crystals and focused at ~1 μm spot size. Unless stated otherwise, the maximum power output of the laser source was filtered to 0.01% of the maximum power output.

Thin-film deposition: A POLOS spin coater was inside a nitrogen-filled glove box. The thin film substrates were made of glass with a thin layer of FTO at one side, at a size of 1.5x1.5 cm and left to clean in a solution for 3hours and then rinsed (water and ethanol) and dried in the 70℃ for 30 minutes. A 100μL pipet was used to apply the product (20mg of each compound dissolved in 50μL of DMF) on the substrate. The spin coater is started using a pre-recorded program of two steps, containing the speed increases, speeds and time of each part. The first step was programmed to have max speed of 6000 rpm with acceleration at 200 rpm/s for 10.0 ss.s. The second step was programmed to have max speed of 6000 rpm with acceleration at 6000 rpm/s for 20.0 ss.s. The substrate was collected and placed at a hot plate for annealing at 120°C for 30 minutes (DMF).

Chapter 1

RESULTS AND DISCUSSION

Synthesis of the 2D Double Halide Perovskites

The first system of study related to the previous experimental work of our group, on the synthesis and characterization of lead-free, 2D, hybrid halide perovskites. That system concerned mixed-metal Ag-In, Ag-Bi and Ag-Sb halide, layered perovskites, with (4-aminomethyl) piperidinium (4-AMP) as the spacer cation. This system proved to host water molecules within the perovskite structure voids and served as the inspiration of the new set of layered, mixed-metal double halide perovskites studied during my graduate studies. The new dication used (2-halopropane-1,3-diamonium dihalide, DicX, X = Br, I), aimed to test two new reaction systems, and address the influence of the organic halide in the interlayer with the perovskite layers.

Initially, the synthesis of the $(DicBr)_2AgBiBr_8$ perovskite was pursued, targeting a composition where the ordering of Ag^+ and Bi^{3+} could stabilize a double perovskite. We selected 2-bromopropane-1,3-diamonium dibromide ($(DicBr)^{2+}$ $2Br^-$) dication as a suitable spacer to generate a 2D structure, due to the extra Br atom in order to check how that extra bromide in the organic part could affect the properties of a double perovskite.

The synthesis reaction proceeds smoothly, by successful dissolution of the metal and the organic precursors ($AgNO_3$ first followed by $BiBr_3$ and the $(DicBr)^{2+}$ addition) in 2.5 pipets of the acidic aqueous medium producing a clear yellow solution. In order to minimize the loss of the reactant, the reaction vessel was immediately covered after the additions, and the solution was heated up to reach a boiling temperature. At this temperature (~150 ^oC), using the glass cover as a condensation surface, the reaction mixture was left under reflux condition for 10-15 minutes, in order to reach a thermodynamic equilibrium. After the reaction deemed to be complete, stirring and heating were discontinued and the reaction was left to cool slowly to ambient temperature, using the glass cover to maintain the equilibrium conditions. Upon cooling, yellow, small, plate-like crystals began to precipitate. The precipitation was complete in ~30min after which the solid was filtered and cleaned with acetone, and in order to dry, the sample was left in the oven at 70 ^oC to heat for 20 minutes. The procedure was repeated for the $(DicBr)_2AgSbBr_8$ perovskite for which $BiBr_3$ was replaced by $SbBr_3$. The procedure was similar for these two perovskites, with the difference being that the Sb derivative being more soluble than the Bi one and thus precipitating faster during the crystallization process (equations (1) and (2).

- $2[(\text{Dic Br})\ 2Br] + AgNO_3 + BiBr_3 \xrightarrow{conc.HBr} (DicBr)_2AgBiBr_8$ (1)

and

- $2[(\text{Dic Br})\ 2Br] + AgNO_3 + SbBr_3 \xrightarrow{conc.HBr} (DicBr)_2AgSbBr_8$ (2)

The same procedure was followed for the synthesis of the "$(DicI)_2AgBiI_8$" and "$(DicI)_2AgSbI_8$" perovskite, replacing the acidic solution with concentrated HI solution. The 1D $(DicI)BiI_5$ and $(DicI)SbI_5$ compounds were precipitated instead precipitated instead. The same experiments were conducted by adjusting the concentration of the solution, but every time the 1D compounds would precipitate, proving that double perovskites with silver are not stable in HI acid, as Ag^+ cannot enter the structure, or that the solubility product of the nitrogen halide salt is too high (equations (3) and (4).

- $[(\text{Dic I})\ 2I] + AgI + BiI_3 \xrightarrow{conc.HI} (DicI)BiI_5$ (3)

and

- $[(\text{Dic I})\ 2I] + AgI + SbI_3 \xrightarrow{conc.HI} (DicI)SbI_5$ (4)

To confirm the success of the synthesis and to determine the crystal structure of the product powder X-Ray diffraction patterns were obtained. The materials obtained for the 2D and 1D perovskites are exceptionally pure as judged by X-ray diffraction (XRD) (**Figure 1a-d**), as all experimental patterns agree with the calculated ones. Comparing the calculating with the experimental powder patterns we observe that the PXRD for the 2D $(DicBr)_2AgBiBr_8$ and $(DicBr)_2AgSbBr_8$ compounds, are identical, as are the 1D $(DicI)BiI_5$ and $(DicI)SbI_5$ perovskite reaction products. For both 2D double perovskites there is a strong characteristic peak right before $2\theta = 10°$, corresponding to the (200) plane, while there is a relatively small peak at $\sim 2\theta = 10°$, corresponding to the (111) plane. Also, there is an intense characteristic double peak at $\sim 2\theta = 15°$, corresponding to the (020) and (002) planes, respectively. The reason why some peaks seem to be missing from the experimental PXRD of the $(DicBr)_2AgSbBr_9$ compound, is because the crystals appear to have some degree of preferential orientation (**Figure 1b**). For both 1D perovskites, a weak peak appears right before $2\theta = 10°$, corresponding to the (011) plane, while there is a weak double peak right after $2\theta = 10°$, corresponding to the (002) and (001) planes, respectively. Also, there is a characteristic weak peak right before $2\theta = 15°$, corresponding to the (020) planes.

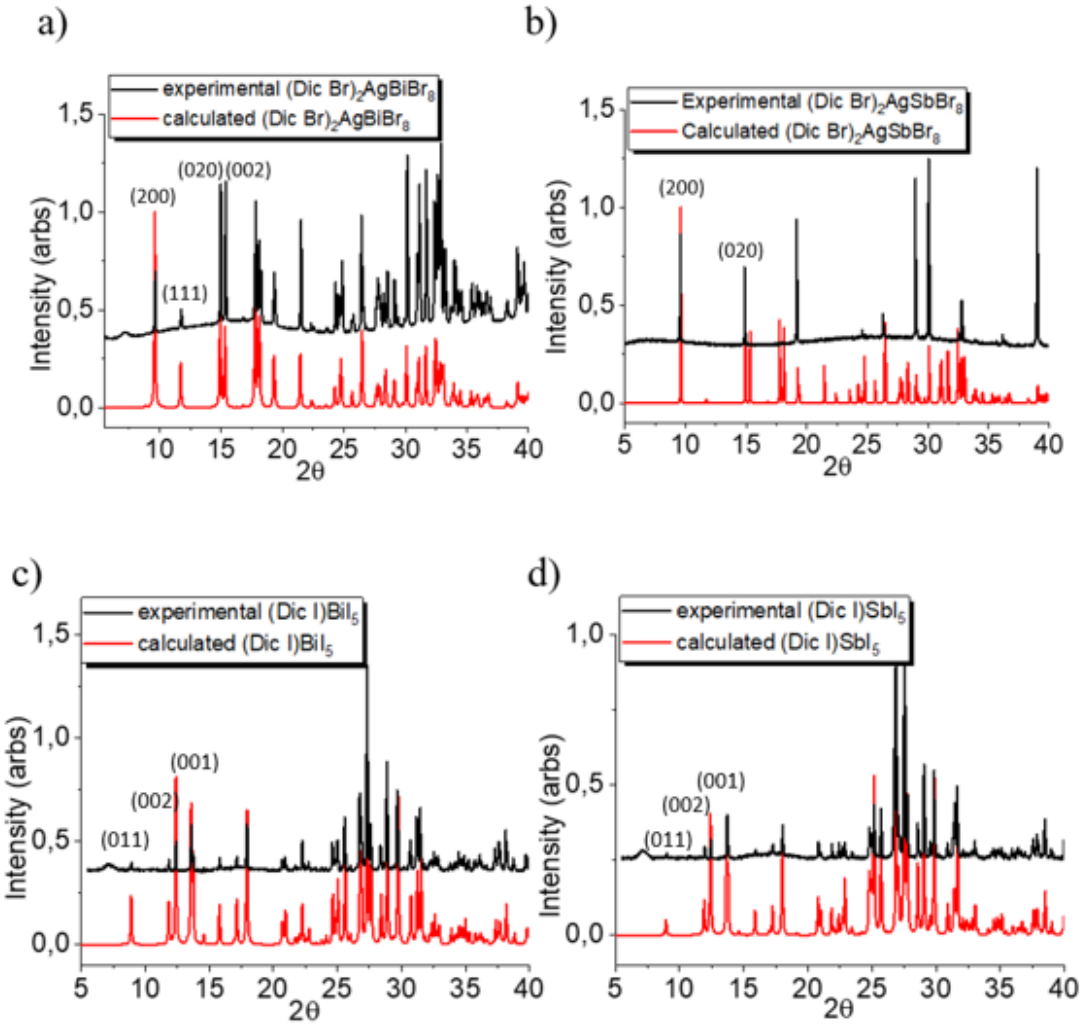

Figure 1. Powder X-ray diffraction (PXRD) patterns of the experimental 2D a) $(DicBr)_2AgBiBr_8$ b) $(DicBr)_2AgSbBr_8$ and 1D c) $(DicI)BiI_5$ and d) $(DicI)SbI_5$ perovskite compounds compared to their calculated patterns.

In order to confirm the success of the synthesis and in order to estimate the thermal stability of the materials, we performed thermogravimetric analysis (TGA) experiments on all the double 2D and 1D hybrid perovskites, as well as DSC measurements to look for potential phase transitions in the -80-200ºC temperature range. The DSC diagrams for the 2D and 1D compounds, are shown in (**Appendix**, **Figures S1a-d**). All the diagrams depict irreversible exothermic processes upwards. No phase transitions between 25°C-180°C were observed. Neither endothermic nor exothermic peaks were observed for any of the n compounds.

The TGA analysis for the 2D double and 1D perovskites, shown in **Figure 2**. All the thermal diagrams for the 2D double perovskites exhibit very similar trends in the temperatures ~200 and ~650°C. The thermal decomposition starts at ~200 °C, displaying a significant mass loss due to the evaporation of the organic part and the corresponding $M^{3+}I_3$ (M^{3+}= Bi, Sb). For

$(DicBr)_2AgBiBr_8$ (79.03%) and $(DicBr)_2AgSbBr_8$ (78.69%). These correspond to ~2 (DicBr), 4HBr and ~1 $BiBr_3$ or ~1 $SbBr_3$, per formula unit for $(DicBr)_2AgBiBr_8$ and $(DicBr)_2AgSbBr_8$, respectively. At temperatures around 650°C both diagrams display mass loss of AgBr at a percentage of 14.63% and 13.89% for $(DicBr)_2AgBiBr_8$ and $(DicBr)_2AgSbBr_8$, respectively. The thermal diagrams for the 1D perovskites are almost identical as the only difference is in the trivalent metal (Bi^{3+} and Sb^{3+}). Both diagrams exhibit only one curve corresponding to ~1 (DicI), 2HI and ~1 BiI_3 or ~1 SbI_3, per formula unit for $(DicI)BiI_5$ (95.95%) and $(DicI)SbI_5$ (95.76%), respectively. These values correspond well with the expected melting points of the inorganic components and suggest that the thermal decomposition proceeds via the initial decomposition of the organic cation at ~200°C.

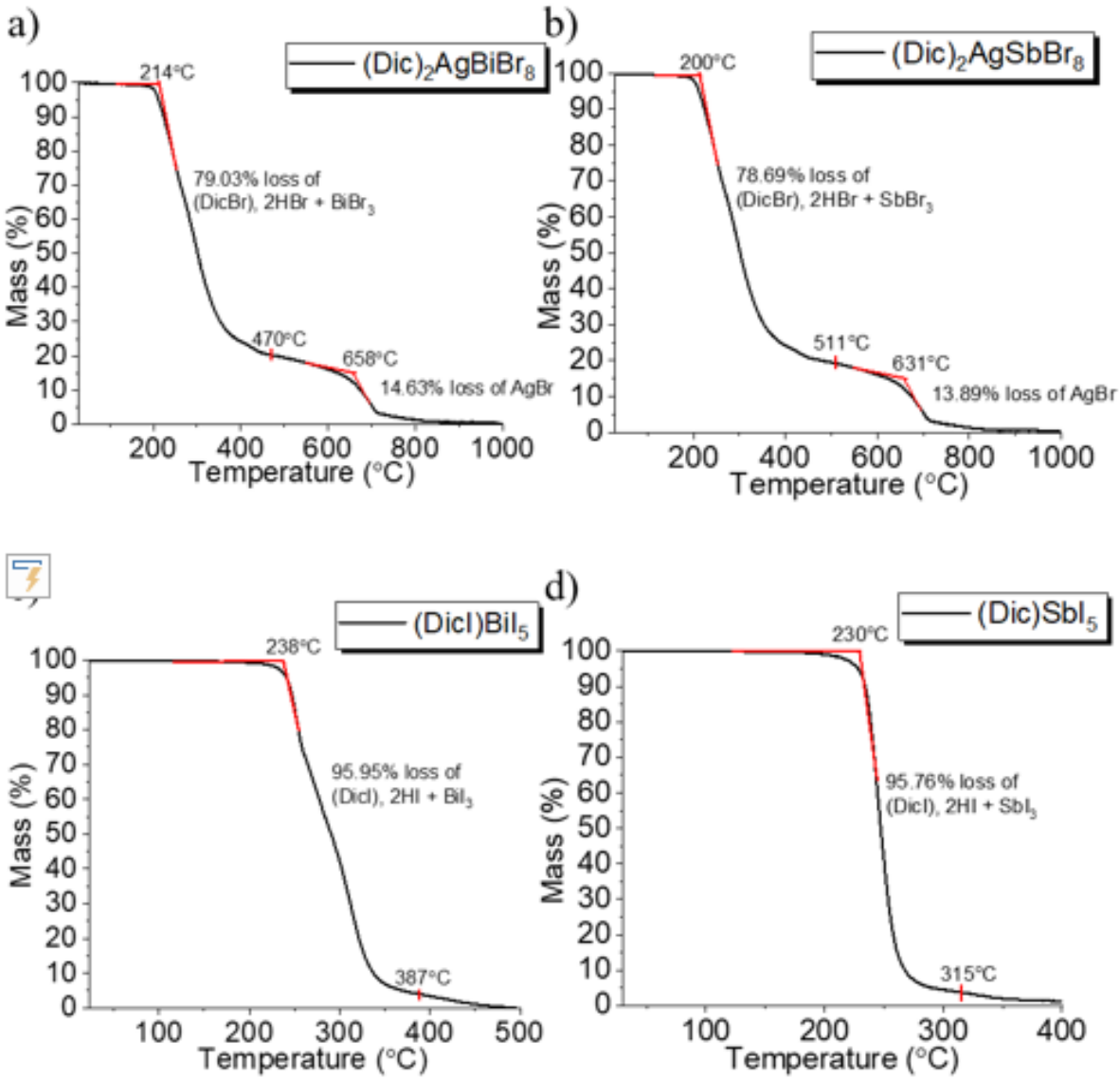

Figure 2. TGA thermograms of the 2D double halide perovskites a) $(DicBr)_2AgBiBr_8$ b) $(DicBr)_2AgSbBr_8$ and of the 1D c) $(DicI)BiI_5$ and d) $(DicI)SbI_5$ perovskites.

Crystal Structure of the 2D Double Halide Perovskites

The crystal structure of the 2D double halide perovskites and the 1D compounds are shown in **Figure 3** and **Figure 4**, respectively. Detailed crystallographic data are provided in the **Appendix**. All the 2D double halide perovskites, $(DicBr)_2AgBiBr_9$ and $(DicBr)_2AgSbBr_9$, crystalize in the centrosymmetric space group *C*2/*c*, while the 1D byproducts $(DicI)BiI_5$ and $(DicI)SbI_5$ crystalize in the non-centrosymmetric space group $P2_12_12_1$. Each perovskite consists of polyhedra that differ from each other in terms of the charge of the central atom, as well as its coordination preference. Although, the main atom for these octahedra varies from Bi to Sb, the atoms occupying the octahedra vertices are Br atoms in all cases. The double perovskites connect in the common motif, where each Ag-centered and each Bi(Sb)-centered octahedron and connected alternately in a perfectly ordered manner to form two dimensional sheets. The organic cation is located in the pockets between the octahedra, linking through each adjacent pair of layers. The organ bromide components are located in the middle of the organic layers, forming short range interactions with the inorganic halide counterparts. The 1D perovskites also form the typical patterns for this structural archetype, with the metal octahedra connected in zig-zag fashion, forming infinite ribbons along the crystal growth direction. Both Sb and Bi counterparts form very similar structures with each other with relatively similar the same lattice parameters. Selected crystallographic information is tabulated in **Table S1**.

The 2D hybrid halide perovskites have general chemical formula of $A_nM^IM^{III}X_8$. The monovalent cation to each perovskite is silver (Ag), while the trivalent cations for each chemical compound separately are bismuth (Bi) and antimony (Sb). The metal arrangement in the crystal structure, is illustrated in **Figure 3**. These perovskites are consisting of two types of regular octahedra. The first kind of regular octahedra consist of an Ag atom surrounded by six Br atoms at its apices. In these octahedra, the two axial Br atoms are equidistant from the Ag atom and form short Ag-Br bonds. By contrast, the four equatorial Br atoms from long Ag-Br bonds, with bond lengths to be approximately the same (**Table S2** in the Appendix). The distortion index for the Ag-Br octahedra is 0.08218 Å and 0.06133 Å, and the bond angle variance is 29.7518° and 18.5197° for $(DicBr)_2AgBiBr_9$ and $(DicBr)_2AgSbBr_9$, respectively, while the distortion index for the M-Br octahedra is 0.00568 Å and 0.02063 Å, and the bond angle variance 0.9214° is and 5.5870° for $(DicBr)_2AgBiBr_9$ and $(DicBr)_2AgSbBr_9$, respectively. Both the distortion index and the bond angle variance of the octahedra were calculated by VESTA[46] using the following equations (5) and (6):

$$\lambda_{oct} = \frac{1}{6}\sum_{n=1}^{6}[(d_n - d_0)/d_0]^2 \qquad (5)$$

$$\sigma^2 = \frac{1}{11}\sum_{n=1}^{12}(\theta_n - 90^{\circ})^2 \qquad (5)$$

Where d_n are the bond distances of Ag-Br and M-Br, d_0 is the average value of the different bond distances and θ_n are the bond angles of Br-Ag-Br and Br-M-Br. The λ_{oct} value of Ag−Br is larger than that of M−Br in both compounds. The same trend is observed for the σ^2 as well.

The second type of regular octahedra consist of a trivalent metal cation (M = Bi^{+3} and Sb^{+3}) surrounded by six Br atoms at its apices. In these octahedra, the two axial Br atoms are nearly equidistant from the M^{+3}, while the four equatorial Br atoms form almost equivalent M-Br bonds, having values, as shown in **Table S2** in the Appendix. The distortion index for these regular octahedra is 0.00568Å and 0.02063Å, for $(DicBr)_2AgBiBr_9$ and $(DicBr)_2AgSbBr_9$, respectively.

Both 2D double halide perovskites display a high degree of out-of-plane tilting of the octahedra along the b axis, while there is no such effect along a and c axes. The average of the out-of-plane Bi−Br−Ag angle being 147.6°, for $(DicBr)_2AgBiBr_9$, while the average out-of-plane Sb−Br−Ag angle for $(DicBr)_2AgSbBr_9$ being 148.6°. Detailed listing of the angles for the in plane and out of plane tilting are shown in **Table S3** of the **Supporting Information**. Between the octahedra we observe that the dications have a periodic orientation with the bromide edges looking at the same direction.

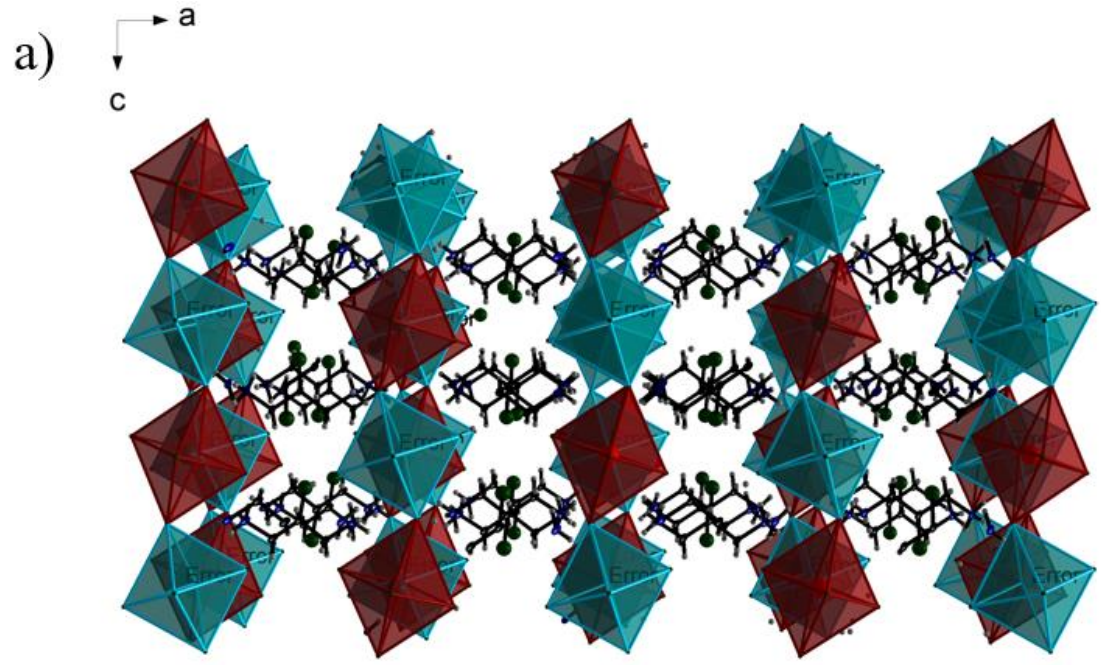

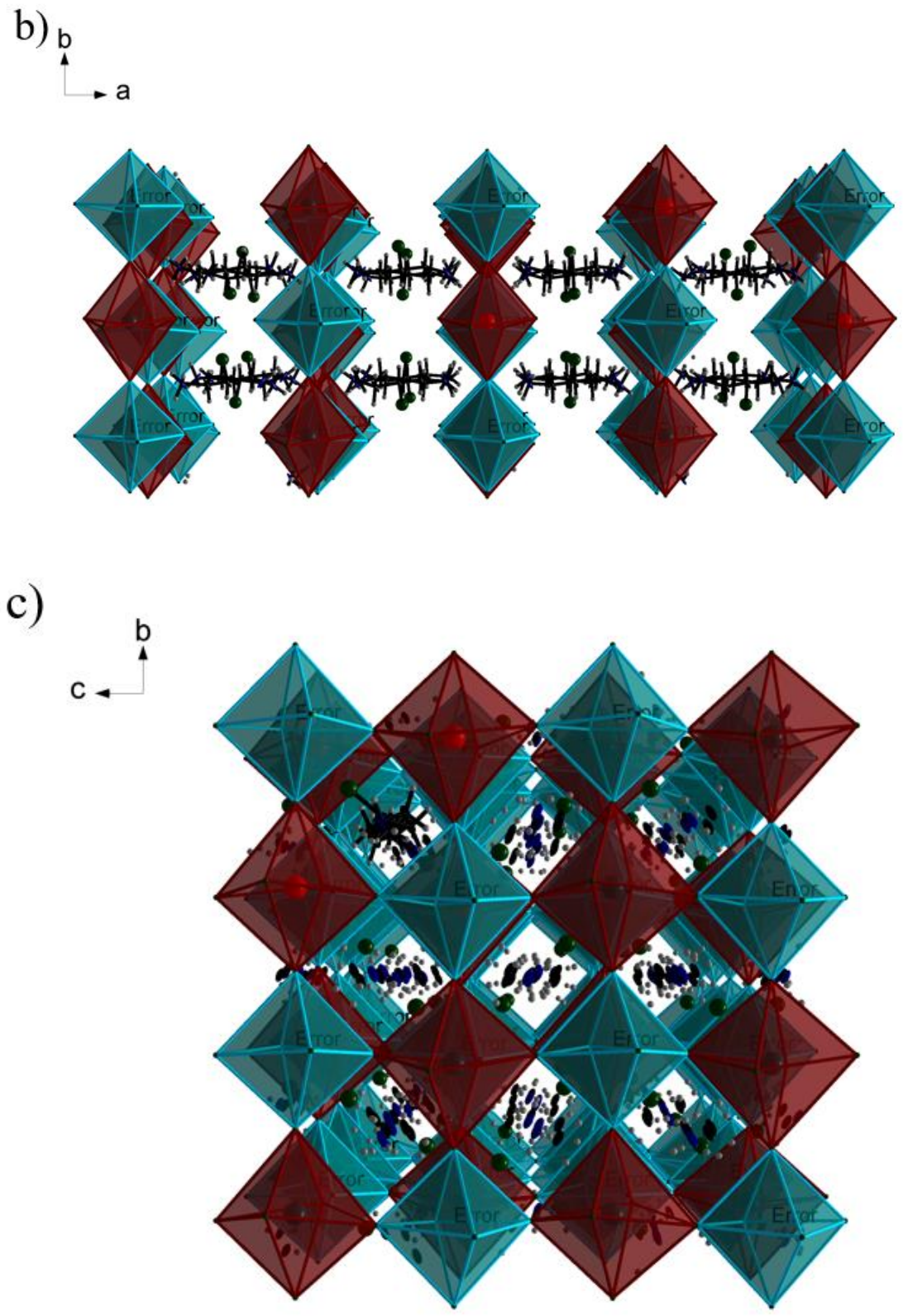

Figure 3. Illustration of the 2D double halide perovskite of $(DicBr)_2AgBiBr_8$ showing the a) tilting along the b axes, b) along the c axes and along the α axes.

In contrast to the layered perovskites, the 1D halide perovskites have general chemical formula of $AM^{III}X_5$. These perovskites are 1D as there is a repeating pattern of two corner-

sharing octahedra connected in zig-zag fashion down the *a* crystallographic axis, without forming any layers and they are inordered. Between the octahedra there are face sharing dications, with their iodide edges being opposite to each other. These perovskites consist of one type of regular octahedron. The trivalent cations for each chemical compound separately are bismuth (Bi) and antimony (Sb), for $(DicI)BiI_5$ and $(DicI)SbI_5$, respectively. The metal arrangement in the crystal structure, is illustrated in **Figure 4**. The octahedron for these compounds consists of a trivalent metal cation ($M = Bi^{+3}$ and Sb^{+3}) surrounded by six Br atoms at its apices. In these octahedra, the two axial Br atoms are nearly equidistant from the M^{+3}, while the four equatorial Br atoms form almost equivalent M-Br bonds, having values, as shown in **Table S2** in the Appendix. The distortion index for these regular octahedra is 0.05651 Å and 0.03651Å, for $(DicI)BiI_5$ and $(DicI)SbI_5$, respectively. Between the octahedra we observe that the dications are facing one another with the organ iodides oriented in opposite directions to one other.

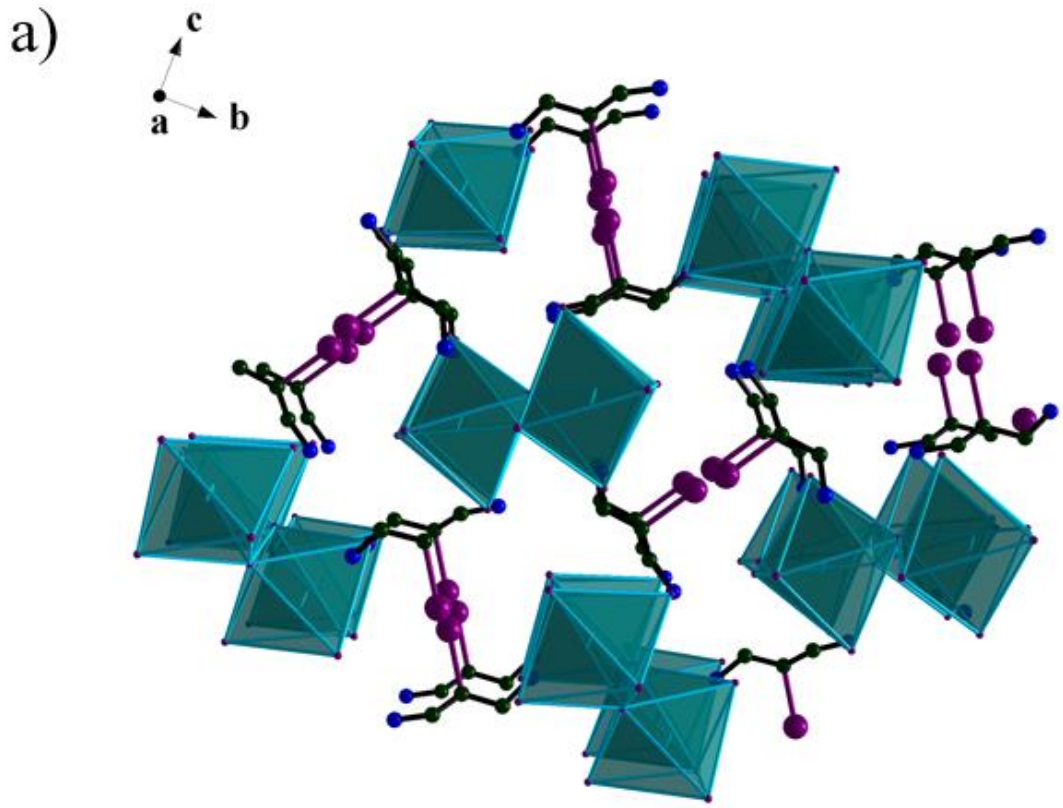

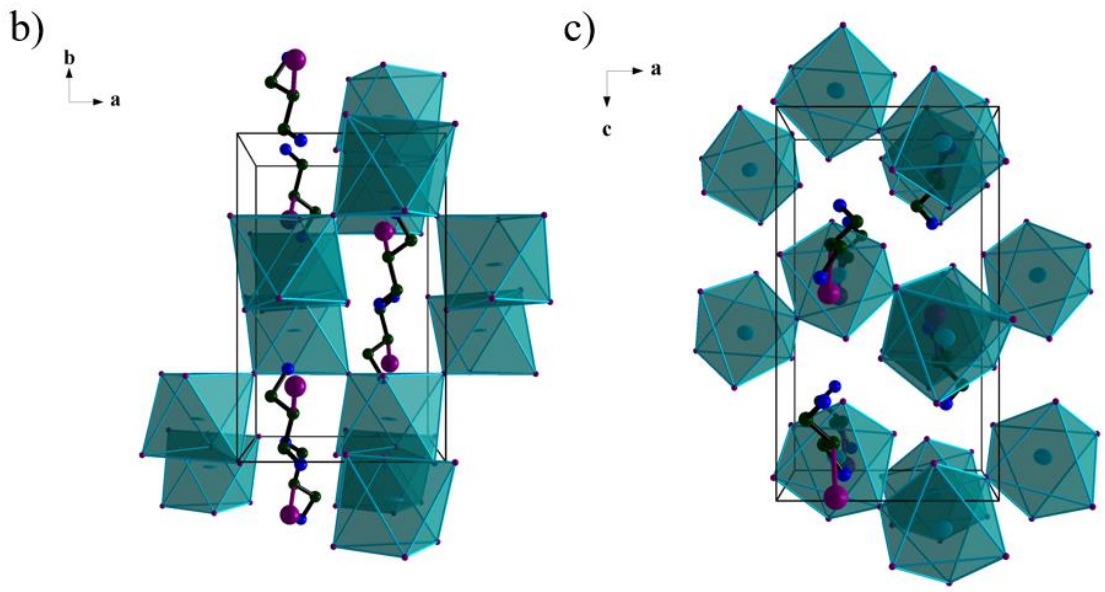

Figure 4. Illustration of the $(DicI)_2BiI_5$ 1D halide perovskite unit cell a) showing the pattern of the octahedra and the organic part, showing the octahedra configuration b) along the c axes and c) along the b axes

.

OPTICAL PROPERTIES

Double Perovskites

In order to estimate the band gap of the new compounds and where they emit in the visible spectrum, we performed diffuse reflectance measurements between 185-1400nm (UV-vis-NIR spectroscopy).

It was found that $(DicBr)_2AgBiBr_9$ and $(DicBr)_2AgSbBr_9$ compounds have similar band gaps of E_g =2.86 eV and E_g = 2.93 eV, respectively, as shown in **Figure 5a**. In good agreement with the observed colors, both compounds have a similar bandgap with Bi slightly narrower than that of Sb. Both of them have a yellow color, with $(DicBr)_2AgBiBr_9$ compound having a lighter color rather than $(DicBr)_2AgSbBr_9$.

For the iodides, the band gaps of $(DicI)BiI_5$, $(DicI)SbI_5$, are E_g = 1.95 eV and E_g = 2.03 eV, respectively, as derived from the spectra shown in **Figure 5b**. As expected, the compounds with iodide have smaller band gap from the 2D perovskites with bromide, and they have darker color.

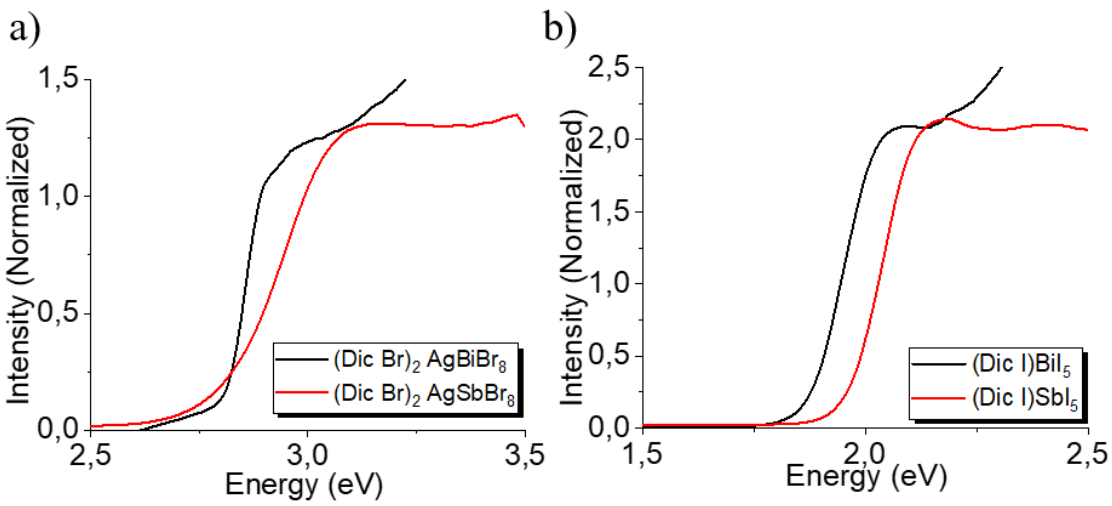

Figure 5. Absorption spectra of the a) 2D double halide perovskites and b) of the 1D compounds, were obtained from diffuse reflectance measurements converted using the Kubelka−Munk function ($\alpha/S = (1 - R)^2 /2R$)[47, 48].

CONCLUSION

The synthesis of Bi/Ag and Sb/Ag-based 2D bromide double perovskites and the synthesis of 1D iodide perovskites promotes the success of obtaining double perovskites when the halide is Br^-. Even though the same experiments were conducted in HBr and HI acid, 1D perovskites with Bi and Sb were obtained in HI. Notably, all the new 2D compounds crystallize in the *C 2/c* space group, while all 1D perovskites were crystalized in $P2_12_12_1$ space group. Both 2D double halide perovskites exhibit out of plane tilting along the b axes and the dications have a periodic orientation with the bromide edges looking at the same direction. In contrast, the 1D halide perovskites appear to have the dications facing one another with the iodides being opposite to each other. The energy gap of the 2D halide perovskites are higher than the ones of the 1D perovskites, but still the energy gap of the Bi compounds have slightly lower energy gap than the Sb compounds.

Chapter 2

RESULTS AND DISCUSSION

Synthesis of the Layered Perovskites

The second part of the study of the organohalide spacer cations, DicX, concerned the synthesis of the layered $(Dic)(MA)_{n-1}Pb_nI_{3n+1}$ homologous series, an ongoing project in the Université d' Angers. Initial experiments succeeded in obtaining the structures of n=1-5 but not as pure phases of them. The synthesis of the pure phases of n=1-3 was the objective of the present chapter, together with the initial experiments to fabricate thin films from the pure materials. The interest of these new compounds lay in the short distance between the perovskite layers, resulting in a possible charge transport perpendicular to the perovskite layers which is of high importance for photovoltaic applications.

Initially, the synthesis of the layered $(Dic)(MA)_{n-1}Pb_nI_{3n+1}$ perovskite series was pursued using Pb^{2+} and MA^+ as M^{2+} and perovskitizer, respectively, knowing that it can create layers[23, 49-52]. We selected the 2-iodopropane-1,3-diamonium diiodide $[(DicI)^{2+}\ 2I^-]$ dication as a suitable spacer to generate these layered perovskites due to the extra iodides containing at its chemical formula creating short I-I bond distances between the layers, enabling a possible charge transport perpendicular to the perovskite layers. That is promising, mainly for photovoltaic applications, as we could synthesis efficient thin films not only with the 3D counterparts of a compound but with its layered counterparts as well.

The synthesis reaction for n=1 proceeds smoothly, by successful dissolution of the metal precursor (PbI_2 or PbO) and the dication with iodide, in the acidic aqueous medium producing a clear yellow solution. The reaction container was immediately covered after the additions, and the solution was heated up to 130 °C. At this temperature, using the glass cover as a condensation surface, the reaction mixture was left under reflux condition for 10-15 minutes, in order to reach a thermodynamic equilibrium. After the reaction deemed to be complete, stirring and heating were discontinued and the reaction was left to cool slowly to ambient temperature, using the glass cover to maintain the equilibrium conditions. Upon cooling, small, red, plate-like crystals began to precipitate. The precipitation was complete in ~30min. The longer the crystals stayed in the solution the further their transition to the hydrated phase of n=1 (yellow phase), proceeds, as the crystals absorb water from the solution and atmosphere. By the time the vial was left to cool in ambient conditions, an hour later the crystals became orange and after a day, they were completely yellow. The solid was filtered and cleaned with ethyl acetate, and in order to characterize the dehydrated phase of n=1 (red), the sample was left in the oven at 70 °C to heat for 20 minutes till it becomes red again. The hydrated

(yellow phase) n=1 seems to be more stable in the atmosphere than the red phase despite the fact that it seems to be reversible procedure according to the stoichiometric equations (7) and (8)..

- $[(\text{Dic I})\,2\text{I}] + PbI_2 + H_2O \xrightarrow{conc.HI} (\text{DicI})PbI_4 \cdot H_2O$ (7)

and

- $[(\text{Dic I})\,2\text{I}] + PbI_2 \xrightarrow{conc.HI} (\text{DicI})PbI_4$ (8)

In both, n=2 and n=3, the reaction steps were the same. We used two vials for each reaction. In the first one, we added the dication and under constant heating (~130 ^{o}C) and stirring in the hot plate, it became clear. At the same time, we prepared the second vial, in which we added first the metal precursor (PbO), in the acidic aqueous medium producing a clear yellow solution. After the solution became clear, we slowly added the MAI, and made sure that the solution remained clear, because if we had added it fast, $MAPbI_3$ would have been precipitated instantly. The reaction vessel was immediately covered after the addition, and the solution was heated up to 130 ^{o}C. The content of the first vial was then added into our main reaction and using the glass cover as a condensation surface, the reaction mixture was left under reflux condition for 10-15 minutes, in order to reach a thermodynamic equilibrium. After the reaction deemed to be complete, stirring and heating were discontinued and the reaction was left to cool slowly to ambient temperature, using the glass cover to maintain the equilibrium conditions. A day later, scarlet, plate like crystals (n=2) and dark-red, plate like crystals (n=3), were starting to form respectively for each synthesis. The crystals were filtered as well as dried in the oven for 10 minutes at 70 ^{o}C, for the solvent to evaporate completely, according to the non-stoichiometric equations (9) and (10).

- $0.25(\text{Dic I})\,I_2 + 1.5PbO + 1(MAI) \xrightarrow{conc.HI} 0.1(\text{DicI})(MA)Pb_2I_7$ (9)

and

- $0.1(\text{Dic I})\,I_2 + 2PbO + 2(MAI) \xrightarrow{conc.HI} 0.1(\text{DicI})(MA)_2Pb_3I_{10}$ (10)

Interestingly, the above procedure is an efficient and conveniently used method in order to obtain the 2D perovskite members (n = 2, 3) in their pure phase, which cannot be obtained when the reaction is done stoichiometrically[19, 22, 23, 53, 54].

To confirm the success of the synthesis and to determine the crystal structure of the product, powder X-Ray diffraction patterns were obtained. The materials obtained for the hydrated n=1 and all the n compounds are exceptionally pure as judged by X-ray diffraction (XRD) (**Figure 7** and **Appendix**). All experimental patterns agree with their calculated ones. The hydrated (yellow) and the dehydrated (red) patterns of n=1, prove that we have two

different phases of n=1 as the two compounds have peaks at different angles than the hydrated ones, having more peaks between 2θ = ~8° to ~15° due to the low dimensionality of the structure, which means that the structure has a lower symmetry and extra crystallographic planes due to crystalline water molecules. Comparing the powder patterns for n = 1-3, we observe that all patterns exhibit peaks in different angles. For the dehydrated n=1, a small characteristic peak shows up right before 2θ = 10°, corresponding to the (200) plane, while there is an intense double peak right before 2θ = 16°, corresponding to the (020) and (002) planes, respectively. For n=2, some peaks including the first one (right after 2θ = 5°, corresponding to (001) crystallographic plane), are not observed in the experimental pattern due to their low signal-to-noise ratio. An intense peak shows up right after 2θ = 10°, corresponding to the (002). We also observe an intense double peak right before 2θ = 15°, corresponding to the (020) and (200) planes. For n=3, we observe a characteristic slightly weak diffraction right before 2θ = 10°, and an intense peak right above the same angle, corresponding to the (004) and (113) planes, respectively. A characteristic double peak is observed at the PXRD of n=3 as well, right before 2θ = 15°, corresponding to the (020) and (115) planes, respectively. The intensity of the peaks comparing to the calculated PXRD it's due to preferential orientation of the crystals (**Appendix**, **Figures S2 a-c**). As shown in **Figure 7**, we managed to obtain the pure phase of the compounds without any traces of $MAPbI_3$.

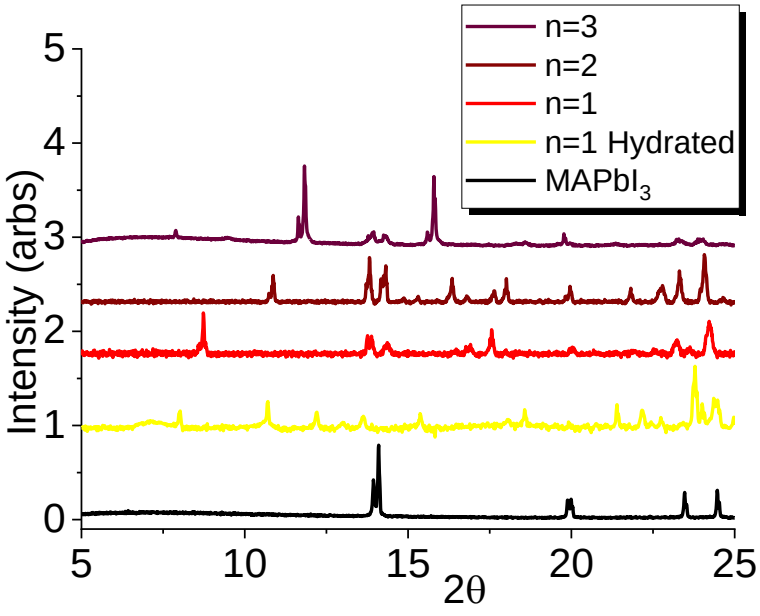

Figure 7. Powder X-ray diffraction (PXRD) patterns of all n compounds of the $(Dic)(MA)_{n-1}Pb_nI_{3n+1}$ series, in comparison with $MAPbI_3$.

In order to confirm the presence of crystalline H_2O in the yellow phase of n=1 and also in order to estimate the thermal stability of the materials, we performed thermogravimetric

analysis (TGA) experiments on all the n compounds, as well as DSC measurements to look for potential phase transitions. The DSC diagrams for the n compounds, is shown in (**Appendix**, **Figures 3a-c**). All the diagrams depict exothermic processes. The evaporation of water molecules from the structures for the n=1, can be seen in the DSC diagrams as an endothermic peak at around 110.8℃, but no reversible transitions occurred. Neither endothermic nor exothermic peaks were observed for both n=2 and 3 in the examined temperature range

The TGA analysis for all n compounds, is shown in **Figures 8**. All the thermal diagrams exhibit very similar trends in the temperatures ~200 and ~400℃. For n=1 only, a slight weight loss is observed around ~80℃ (1.61 %), which corresponds to ~1 H_2O molecule per formula unit. The thermal decomposition starts at ~200 ℃, with the evaporation of the organic part. For n=1 (53.59%), this corresponds to ~1 (DicI) and 2HI, per formula unit and for n=2 (37.41%) and n=3 (31.53%), it corresponds to ~1(DicI) 2HI and MAI. At temperatures around 400℃, all diagrams display a significant mass loss of PbI_2. For n=1 (52.27%) this corresponds to ~1 PbI_2, per formula unit, while for n=2 (51.44%) and n=3 (60.01%), that corresponds to ~2 PbI_2 and ~3 PbI_2, respectively.

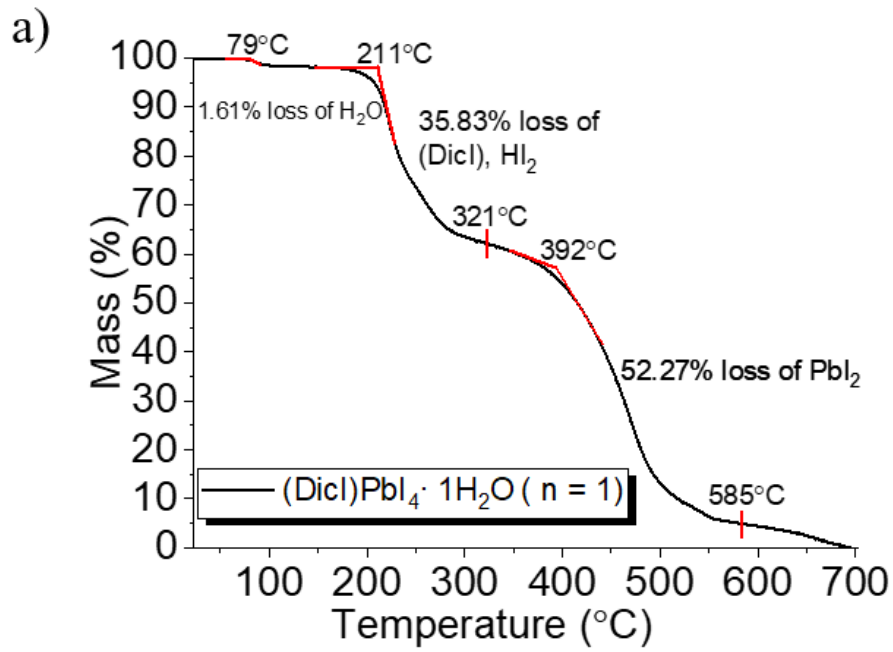

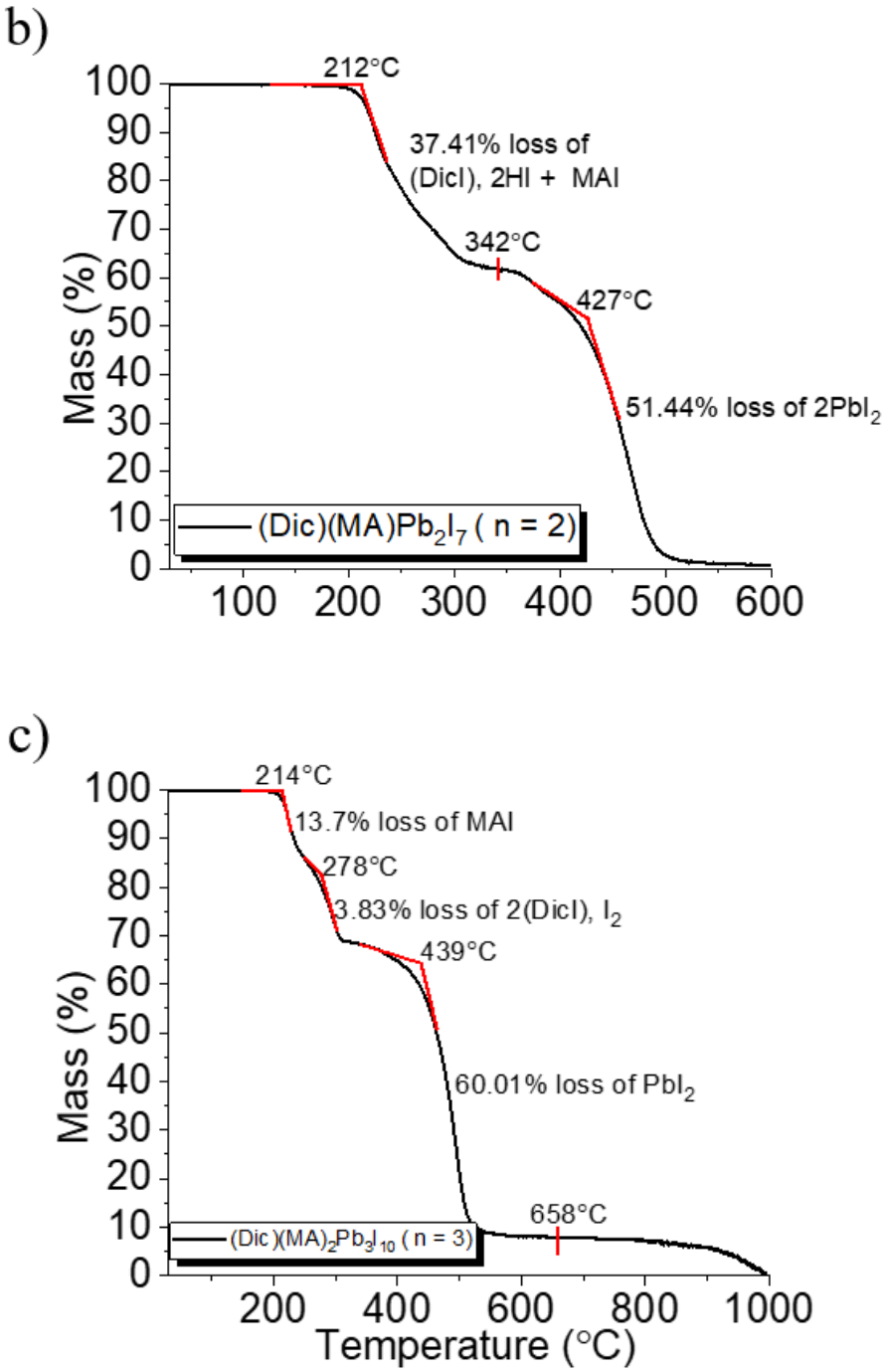

Figure 8. Analysis of n compounds, **a)** between room temperature up to 700 ℃ of the n=1 hydrated compound **b)** between room temperature up to 600 ℃ of the n=2 and **c)** between room temperature up to 1000 ℃ of the n=3.

Crystal Structure of the Layered Perovskites

The crystal structure of the (Dic)$(MA)_{n-1}Pb_nI_{3n+1}$ (n = 1-3) compounds are shown in **Figure 9**, and elected crystallographic information is tabulated in **Table 1**. Detailed crystallographic data are provided in the **Appendix**. All compounds except n=3, have a symmetry that belongs to a space group with an inversion center. The hydrated n=1 crystalizes in the centrosymmetric space group $P2_1/c$, while the n=1 crystalizes in the centrosymmetric space group *Cmce*. The n=2 compound crystalizes in the centrosymmetric space group *Pbam*, and n=3 crystalizes in the non-centrosymmetric space group *Aea*2, with the refinement details and crystallographic data shown in **Table S4**. All parameters are provided in the Appendix. All perovskites from the n series consist of polyhedral that are identical for each compound, as the main atom for these octahedra is Pb^{2+} with iodine atoms occupying the octahedra vertices. These perovskites are considered as Dion Jacobson (DJ), considering the aligning of the octahedra due to the use of a dication cutting along the planes. (**Figure 10**).

Table 1. Crystal Data and Structure Refinement for (Dic)$(MA)_{n-1}Pb_nI_{3n+1}$

	Compounds			
	(DicI)$PbI_4 \cdot 1H_2O$	**(DicI)PbI_4**	**(DicI)(MA)Pb_2I_7**	**(DicI)$(MA)_2Pb_3I_{10}$**
Empirical Formula	$(C_3N_2H_{13}IO_1)$ PbI_4	$(C_3N_2H_{11}I)$ PbI_4	$(C_3H_{11}N_2I)$ (CNH_6) Pb_2 I_7	$(C_3H_{11}N_2I)$ $(CNH_6)_2Pb_3$ I_{10}
Crystal System	monoclinic	orthorhombic	orthorhombic	orthorhombic
Space Group	$P2_1/c$	*Cmce*	*Pbam*	*Aea*2
Unit Cell Dimensions				
a (Å)	a = 6.5423	a = 20.1168(15)	a = 12.3289(8)	a = 12.3926(5)
b (Å)	b = 14.9998	b = 12.6758(10)	b = 12.7636(7)	b = 12.7378(5)
c(Å)	c = 16.7321	c = 12.2263(7)	c = 16.2040(9)	c = 44.8986(15)
α (deg)	α = 90	α = 90	α = 90	α = 90
β (deg)	β = 94.941	β = 90	β = 90	β = 90
γ (deg)	γ = 90	γ = 90	γ = 90	γ = 90
Volume ($Å^3$)	1635.873	3117.7(4)	2793.813	7087.4(5)
Z	4	8	4	8
Density (gr/ cm^3)	3.7958	3.9067	4.0032	4.0426
Independent Reflections	2954 [Rint = 0.1612]	1462 [Rint = N/A]	2398 [Rint = N/A]	6181 [Rint = N/A]
Data/restrains/parameters	2954 / 0 / 109	1462 / 0 / 66	2398 / 0 / 86	6181 / 9 / 176

Final *R* Indices [I>2σ(I)]	Robs = 0.1328, wRobs = 0.1373	Robs = 0.0473 wRobs = 0.0519	Robs = 0.0311 wRobs = 0.0329	Robs = 0.0533 wRobs = 0.1129
R indices [all data]	Rall = 0.1546, wRall = 0.1425	Rall = 0.0652 wRall = 0.0546	Rall = 0.0451 wRall = 0.0349	Rall = 0.0668 wRall = 0.1180
Fourier Difference max and min ($e \cdot Å^{-3}$)	8.94 and -7.26	5.39 and -1.85	4.77 and -1.24	4.78 and -1.72

[a] $R = \sum \| F_o| - |F_c \| / \sum |F_o|, wR = \{\sum [w(|F_o|^2 - |F_c|^2)^2]/\sum [w(|F^\circ|^4)^{1/2} \; and \; w = 1/(\sigma^2 (I) + 0.0004 I^2)$.

The 2-dimensional perovskites from the n series, have the general chemical formula of $(DicI)MA_{n-1}Pb_nI_{3n+1}$. The bivalent cation of each perovskite is lead (Pb). The special feature of the perovskites presented here is that the spacer used to cut the perovskite planes and create the layers, has an extra iodide in its structure, forming short I-I interactions between the organic and inorganic parts of the perovskites. Also, since this is a relatively small cation, the conducting perovskite layers are very close to one another due to Van der Waals interactions between the terminal I^- of the octahedra and the extra iodide on the dication. The distances between the I—I of the organic and inorganic as well as the interlayer distances, get smaller when the number of layers increases as shown in **Table 2**. As a result, a possible charge transport perpendicular to the perovskite layers can occur, making them behave like a 3D perovskite. Each perovskite consists of regular corner sharing octahedra, except the hydrated n=1, which cannot be considered as perovskite. As shown in **Figure 9**, as we can see from the view along the *a*-axis, the octahedra for the hydrated n=1 are connected to each other via their edges, while they appear as corner sharing when viewed along the b axis as shown in **Figure 10**. The central atom for all compounds is a bivalent metal (Pb^{+2}) surrounded by six I^- anions at its apices. In these octahedra, the two axial I^- anions are equidistant from the Pb^{2+} (3.22 Å), while the four equatorial I- anions form almost equivalent Pb-I bonds, having values, as shown in **Table S2** in the Appendix. Only for n=2 and 3 , there is a small monovalent cation (MA^+) occupying the space between the octahedra. The distortion index for these regular octahedra is 0.00895 Å.

All the structures display a high degree of out-of-plane tilting of the octahedra along the b axis, while there is no such effect along a and c axes. While the number of layers increases, the average of the equatorial Pb−I−Pb angles increases being 161.47°, 151.48° and 153.62°, for n= 1, 2 and 3, respectively. Detailed listing of the angles for the in plane and out of plane tilting are shown in **Table S6** of the **Appendix**.

Table 2. I—I Distances between the I of the organic and the I of the inorganic part of the $(DicI)(MA)_{n-2}Pb_nI_{3n+1}$ Perovskites.

	Compounds	I—I Distances Organic-inorganic (Å)	I—I Distances Inorganic-inorganic (Å)
n=1	$(DicI)PbI_4$	3.972	4.033
n=2	$(DicI)(MA)Pb_2I_7$	3.910	3.916
n=3	$(DicI)(MA)_2Pb_3I_{10}$	3.898	3.882
n=4	$(DicI)(MA)_3Pb_4I_{13}$	3.886	3.880

The short interlayer distances between the I—I distances of the inorganic part of the perovskite sheets, were proved once again that occurred due to the new organic dication that we used. Even though there are many dications that are used in order to synthesis Dion-Jacobson perovskites, we selected some of them considering their small size to compare the interlayer distances between the octahedra when each one of them was used compared to the $DicI^{2+}$. As shown in **Table 3**, we exam the I—I distances between the n=1 layers, when different spacers are used. All the displayed dications have interlayer distances between their Pb-I based octahedra that range from ~4.0-4.28 Å, when supposably small dications, like 3AMP[22, 55], 4AMP[22, 23], mPDA[56] and H_2BDA[57, 58] are used. On the contrary, when the $DicI^{2+}$ was used, the interlayer distance seems to be around 3.9 Å.

Table 3. I—I Distances between the iodine parts of lead based octahedra, when different dications are used.

Name Of the Organic Dication	Short Name of the Organic Cation	Chemical Compound	I—I Distances (Å)
2-iodopropane-1,3-diamonium diodide	$DicI^{2+}$	$NH_3^+CH_2CH(I)CH_2NH_3^+$	3.946
3-aminomethylpiperidine	3AMP	$NH_2CH_2CCHNCHCHCHCH$	4.187
4-aminomethylpiperidine	4AMP	$NH_2CH_2CCHCHNCHCH$	4.211
m-Phenylenediammonium	mPDA	$NH_3CCHCHCHCNH_3CH$	4.273
1,4-butanediammonium	H_2BDA	$NH_3CH_2CH_2CH_2CH_2\ NH_3$	4.285

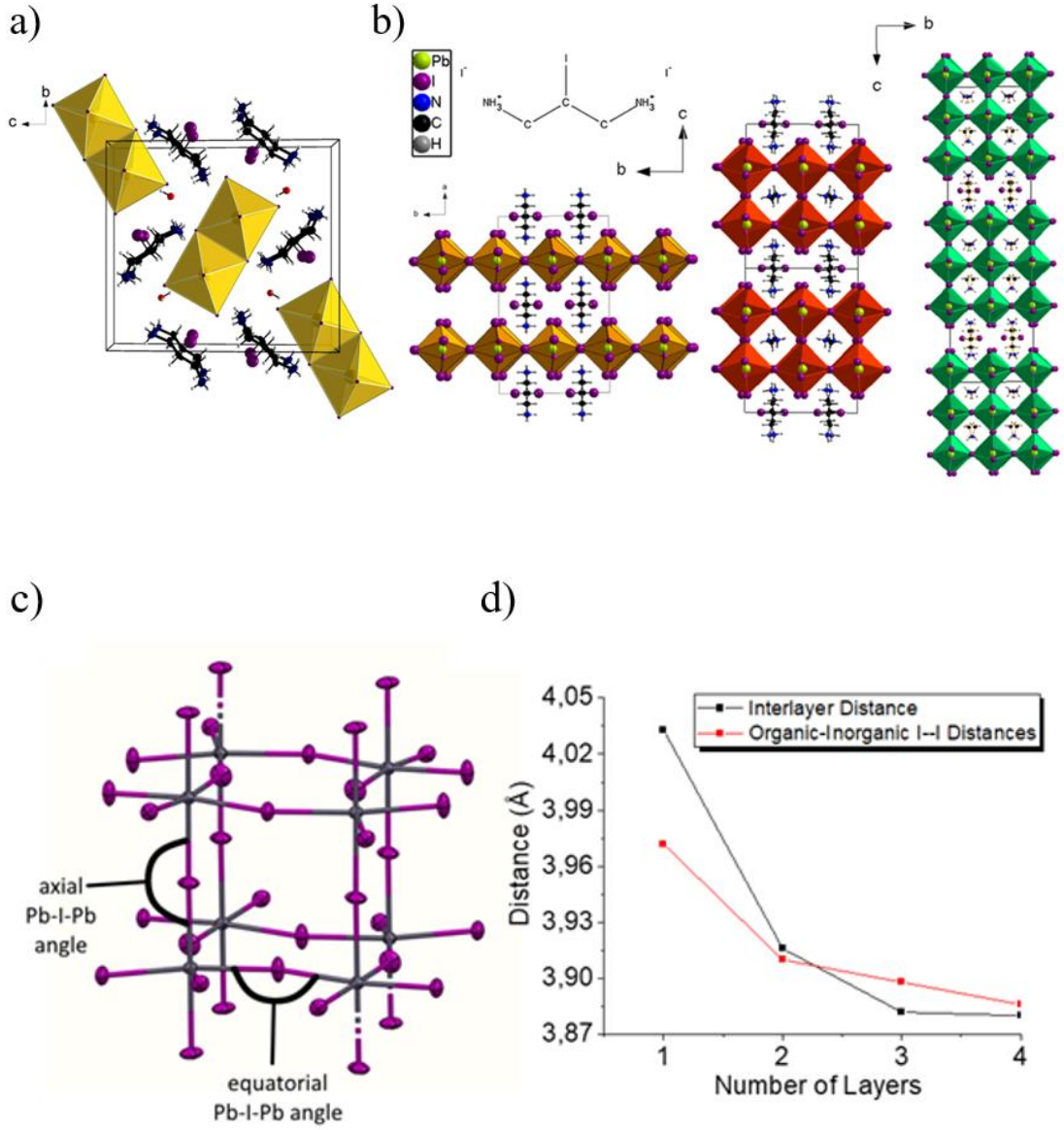

Figure 9. Crystal structures of (DicI)$(MA)_{n-1}Pb_nI_{3n+1}$: a) n=1hydrated, b) n=1-3. The zoom of the spacer part in a). c) Definition of axial and equatorial Pb−I−Pb angles. d) Interlayer and iodide distances between the organic and inorganic components, a function of the number of layers.

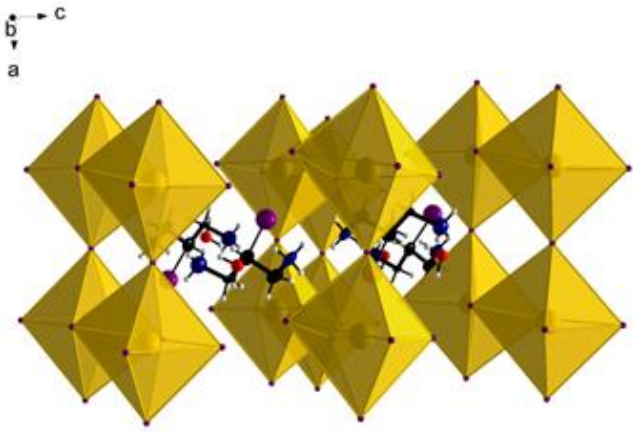

Figure 10. The hydrated n=1 compound, (DicI)$PbI_4 \cdot 1H_2O$, as viewed along the *b*-axis

OPTICAL PROPERTIES

Layered Perovskites

In order to calculate the band gap of the new n series and where they emit in the visible spectrum, we performed diffuse reflectance measurements between 185-1400nm (UV-vis-NIR spectroscopy) and photoluminescence spectroscopy (PL) analysis.

Table 2. Optical Properties and Color of the $(Dic)(MA)_{n-1}Pb_nI_{3n+1}$

	Compounds	E_g (eV)	PL (eV)	Color
n=1 Hydrated	$(DicI)PbI_4 \cdot 1H_2O$	2.48	2.88	Yellow
n=1	$(DicI)PbI_4$	2.12	2.25	Red
n=2	$(DicI)(MA)Pb_2I_7$	1.96	2.09	Scarlet
n=3	$(DicI)(MA)_2Pb_3I_{10}$	1.76	1.97	Dark Red

All layered perovskites consist of alternating perovskite/spacer layers. Their difference in the density of electronic states means that the spacer layers act as potential barriers for the free carriers of the perovskite layers, forming multiple quantum wells in a direction perpendicular to the plane of the layers[59]. The grater the thickness of the perovskite layer, the greater the length of the quantum well (**Equation 1**). The length of the well is inversely proportional to the energy gap, which is therefore inversely proportional to the square of the number of layers, resulting to higher wavelength absorption, the higher the number of layers is. This relationship can be surmised by the following formalization (Equations 11 and 12):

$$E = \frac{\hbar^2 n^2 \pi^2}{2mL_z^2} \qquad (11)$$

$$n_{layers} \propto L_z \qquad (12)$$

where n is the excitation state of the electron, m the electron mass and $L_z$is the quantum thickness proportional to the number of layers[18, 60].

Having defined that, it's easy to understand the behavior that we observe in the absorption spectra of **Figure 11**, with the energy gap increasing as the number of layers decreases (**Table 2**). We observe that the n=1 hydrated exhibits an energy gap at 2.48 eV compared to the dehydrated n=1, which exhibits smaller energy gap at 2.12 eV. Since the hydrated structure of n=1 comprises of 1D perovskite nanowires, it exhibits quantum confinement of greater order and therefore is expected to have a larger energy gap compared to

its 2D counterpart. The energy gap of n=2 exhibits band gap at 1.96 eV, while n=3 and $MAPbI_3$ exhibits band gap at 1.76 eV and 1.55 eV, respectively, which confirms the expected trend. As also expected, the 3D $MAPbI_3$ compound exhibits the lowest energy gap, as it is representing the n=∞ number of layers. The spectra for all n compounds show one pronounced curve each, which serves as evidence for the purity of our compounds.

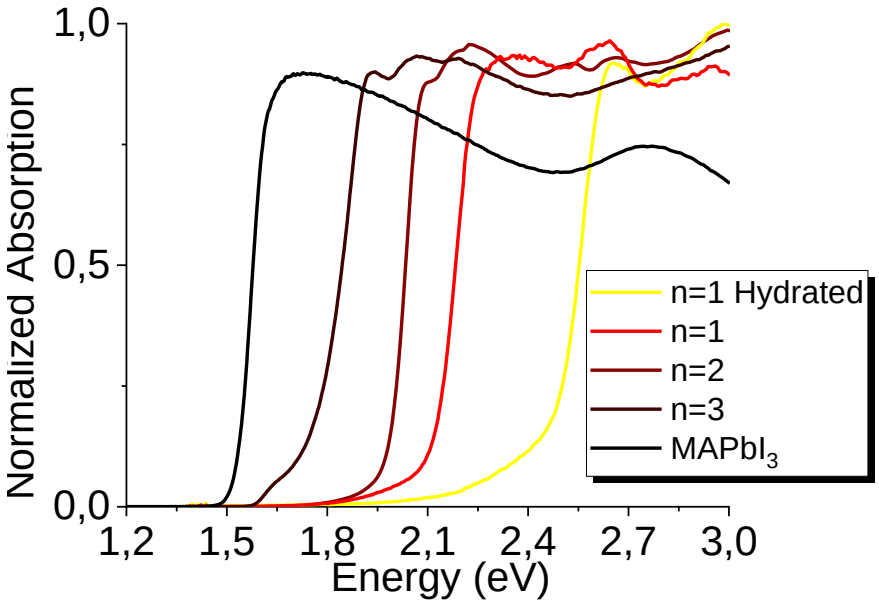

Figure 11. Absorption spectra of the n series and $MAPbI_3$, were obtained from diffuse reflectance measurements converted using the Kubelka–Munk function ($\alpha/S = (1 - R)^2 /2R$)[47, 48].

Photoluminescence properties of specimens obtained from all n compounds, as shown in **Figure 12**. were measured at room temperature using a confocal microscope setup with a steady-state excitation source (λ_{exc} = 473 nm). The photoluminescence emission energy of all the 2D perovskites described here decreases with increasing layer thickness similar to the band gap trend (**Table 2**). The photoluminescence spectra consist of one single emission peak for each of the compounds corresponding to the absorption spectra. The n compounds emit between 500 and 700 nm, while the n=1 hydrated emits between 350 to 600nm. A sharp, weak PL emission was observed for all of the compounds at 430nm, 550nm, 593nm and 630nm, for n=1hydrated 1, 2 and 3, respectively. The emission wavelength is consistent with the experimentally determined band gaps providing further evidence for the direct nature of the band gap. Also, edge effect was observed for all compounds except n=1 hydrated and dehydrated, at 742nm which corresponds to the bulk material's emission ($MAPbI_3$) as previously reported[22, 61-63]. (**Supporting Information**, **Figures S4 a, b**).

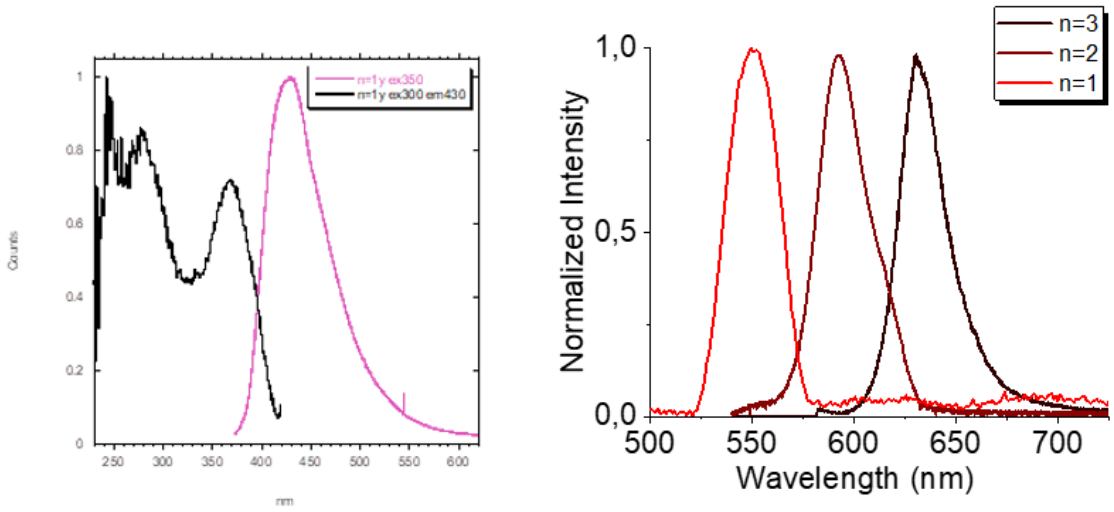

Figure 12. Photoluminescence spectra at the right-side showing PL and PLE of n=1 hydrated compound, while on the left-side showing PL spectra of n=1-3.

Band Structure

DFT calculations for (Dic)$(MA)_{n-1}Pb_nI_{3n+1}$ (n = 1-3) compounds have been made in order to determine the energy bands, as shown in **Figure 13**. The band dispersion for the n=1-3 compounds, along the GM→Z direction already indicates a very effective interlayer electronic communication. This makes sense considering the short interlayer distance and the established active role of the extra iodine from the organic molecule. Also, along the GM→Z direction the conduction band edge is flattened, indicating bulk like behavior mostly for the n=1 compound. That is an unusual behavior as we compared our results with the DFT results of BA_2PbI_4[64], which displays clear parabolic band edges at the Γ point of the Brillouin zone.

All compounds exhibit direct band gap at the GM point of the Brillouin zone, which becomes narrower as the number of layers increases, following the trend of the UV and PL measurements. Also, as the number of layers increases the band dispersion becomes more pronounced.

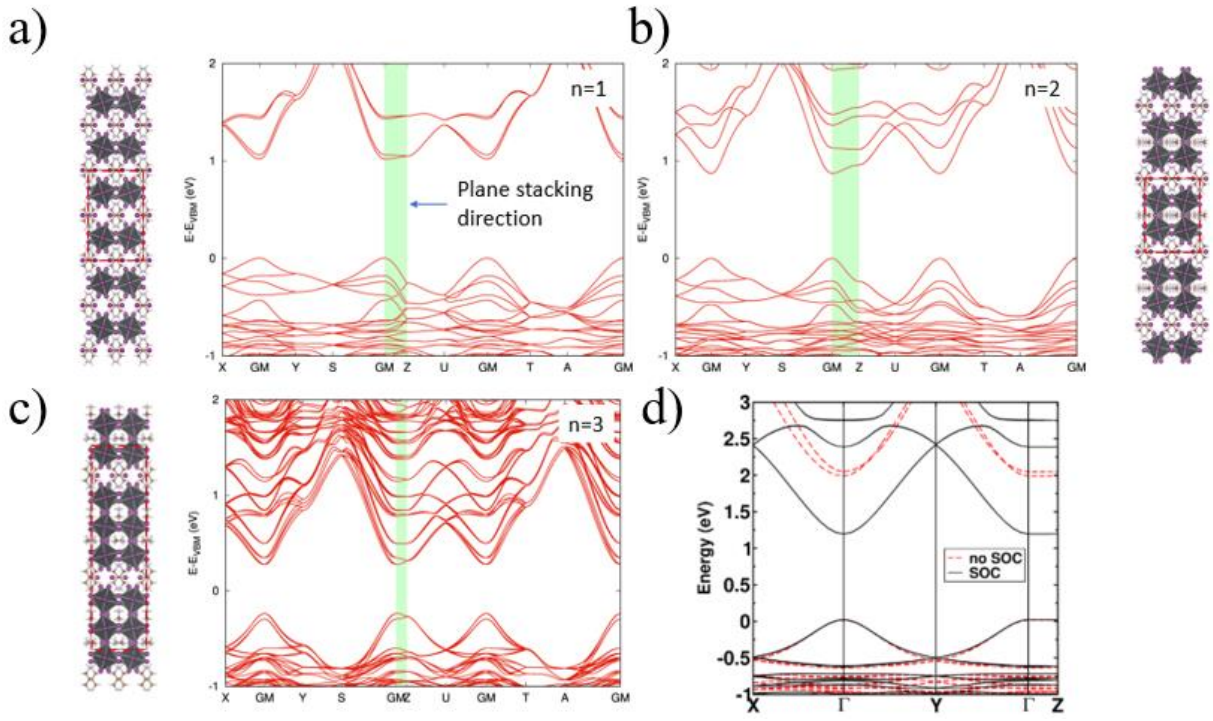

Figure 13. DFT calculations of energy bands for the a) n=1, b) n=2, c) n=3 members of the (DicI)$(MA)_{n-1}Pb_nI_{3n+1}$series and d) the n=1 of the BA_2PbI_4.

The electronic behavior of the compounds is highly unusual, since there are no observed flat bands corresponding with the cross-plane direction. Based on this, it is possible to suggest that the presence of the organ iodide pseudo layer within the quantum-well barrier, in close proximity to the quantum wells, does indeed succeed in

"penetrating" through the boundaries and generates a unique charge-transport pathway. This change, together with the drastic change of the dielectric contrast between the inorganic and organic layers provides a very different electronic landscape compared to most 2D perovskites reported to date and may hold great promise for application of the materials in photovoltaics.

CONCLUSION

A new homologous series have been synthesized and characterized. The synthesis of $(Dic)(MA)_{n-1}Pb_nI_{3n+1}$ (n = 1-3) homologous series using a new dication with an extra iodide at its structure, promotes a new type of compounds that has the ability to resemble bulk materials. The extra iodide in the formula results in short, I-I distances between the layers, enabling a possible charge transport perpendicular to the perovskite layers. While all perovskites of this series appear to be stable in ambient conditions, n=1 is sensitive and seams to absorb water molecules from the atmosphere, resulting in phase transition. (From red they became yellow) This transition is reversible, when the crystals are under heat they return to their original state. All the compounds are direct narrow bandgap semiconductors with bandgaps between 2.48 eV (n=1) – 1.50 eV ($MPbI_3$). As it was expected, the energy gap increases as the number of layers decreases ($Eg_{hydrated,\ n=1} > Eg_{n=1} > Eg_{n=2} > Eg_{n=3}$). Thin films of the homologous series were synthesized using spin coating method and characterized via XRD. Successful was the synthesis of n=1 and in some cases for n=2 as well. For n=3, $MAPbI_3$ was mainly obtained.

The unpredictable physical properties of the $(Dic)(MA)_{n-1}Pb_nI_{3n+1}$ (n = 1-3) homologous series reported here open new window towards the discovery of new materials of this family so that a better understanding of the electronic properties of these fascinating materials can be achieved.

Chapter 3

Thin Film Fabrication and Characterization of the Layered Perovskites.

Solid-state solar cells have triggered a phenomenal advance in the photovoltaic efficiency the past few years[19, 65-70]. The best photovoltaic efficiency of 26.03% for perovskite solar cells has been certified by NREL[69, 71], while the most prominent choice among the light absorbers so far is methylammonium lead iodide ($MAPbI_3$)[72-74].

In order to test if the 2D $(Dic)(MA)_{n-1}Pb_nI_{3n+1}$ family of perovskite compounds (n = 1−3), would be of any use in photovoltaic applications we fabricated thin films. As evident form the absorption spectra, the compounds with more layers absorb a larger range of the visible spectrum. Also, the fact that the iodide of the organic dications may assist charge transfer between the layers, means that the members of this homologous series are good candidates for use as photovoltaic materials.

In this work, all perovskite films were fabricated by a two-step deposition method, by means of spin-coating the DMF precursor solutions of perovskite on the FTO part of the glass substrates and after that, the substrates were placed at a hot plate for annealing at 120°C for 30 minutes. The materials deposited on the thin films were synthesized from a stoichiometric reaction with three different ways, between PbI_2, MAI, and 2-iodopropane-1,3-diamonium diiodide $[(DicI)^{2+}\ 2I^-]$. All the solutions that were obtained before spin coating were yellow, as well as the films. However, they changed color during the thermal annealing process.

The first batch of films was made by preparing precursor solution, for all the n compounds, by dissolving 20 mg of the compound we wanted in 50 μL of DMF. In the cases of n=2 and n=3, they compounds didn't dissolve easily, so heating at 100°C till a clear solution was obtained (1-2 min) was a necessary step.

The second batch of films was made by preparing precursor solution, for all the n compounds, by mixing a stoichiometric 1:2 and 2:3 molar ratio of MAI and PbI_2 in DMF, for n=2 and n=3 respectively. For n=1 we mixed a 1:1 molar ratio of $[(DicI)^{2+}\ 2I^-]$ and PbI_2 in DMF. The amount of $[(DicI)^{2+}\ 2I^-]$ that we used in order to synthesis the precursor solution was always 1 equivalent. All reactions used 1M solution of PbI_2 in 100 μL of DMF, the concentration of which was used as a reference point for the calculations of the relevant amounts of each reagent.

The third batch of films was made by preparing precursor solution, for all the n compounds, by mixing a stoichiometric 1:1 and 1:2 molar ratio of n=1 crystals and $MAPbI_3$ in 50 μL of DMF.

In order to confirm the success of the synthesis, powder X-Ray diffraction patterns were obtained. The XRD from all the films were compared to their calculated powder-XRD patterns in order to see which batch was more successful and able to identify whether we were able to deposit the pure n=2 and 3 in thin film.

The XRD patterns for n=1 dehydrated show that we succeeded to synthesize thin films with that phase, using reagents or yellow crystals. As expected, in both cases the films changed color from yellow to orange/red when treated thermally at 100°C. (**Appendix**, **Figure S5a**) In the case of n=2, the first batch (dissolved n=2 crystals in DMF, light brown) showed almost the same results as the third batch (1:1 molar ratio of n=1 crystals and $MAPbI_3$, dark brown), with the first batch having an extra pick at 8.78Å belonging to n=1. The second batch (stoichiometric use of the reagents for n=2, dark red) seams to give us an extra pick of PbI_2 at ~12.70Å, and to have traces of $MAPbI_3$. All films seem to have peaks corresponding to the calculated PXRD of the n=2 compound, and even though the third batch seems to correspond better to the PXRD (not extra peaks), the second batch appears to have the color we would expect (dark red). (**Appendix**, **Figure S5b**) In the case of n=3, we were not able to fabricate any pure film, from any of the batches, as we observe only $MAPbI_3$ peaks in all of the XRD patters. (**Appendix**, **Figure S5c**)

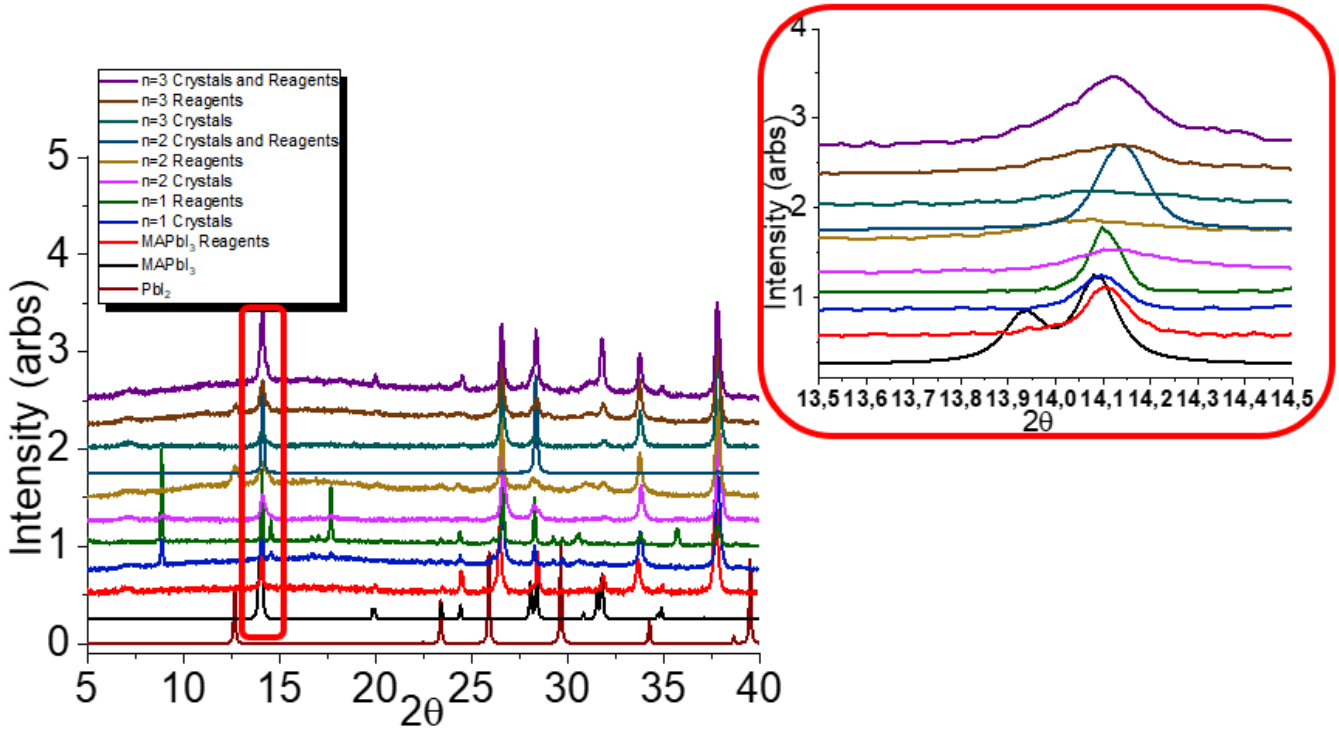

Figure 14. All the Powder X-ray diffraction (PXRD) patterns of all the n film compounds comparing them with $MAPbI_3$ and PbI_2.

OPTICAL PROPERTIES

The fabricated thin films where further characterized. Reflectance measurements were made for all the n series films and only the ones shown in Figure **15** gave us good results. Also, what we observe from the spectra is that only the n=1 films were purely made, as a main peak is observed around 530nm. The n=2 film that was made using only reagents, resulted to be a combination of n=1, 2 and $MAPbI_3$, as peaks at around 530nm, 570nm and 610nm are observed. The n=2 film that was fabricated using n=1 crystals and reagents in the right stoichiometry depict only one curve, which probably corresponds to n=3 or n=1. For the n=3 film that was fabricated using only reagents in the correct stoichiometry, two peaks are observed, with the first one corresponding to n=2 and the second one corresponding to $MAPbI_3$, while for the n=3 film using the combination of n=1 crystals and reagents, two peaks appear as well, with the first one corresponding to n=1 and the second one to $MAPbI_3$.

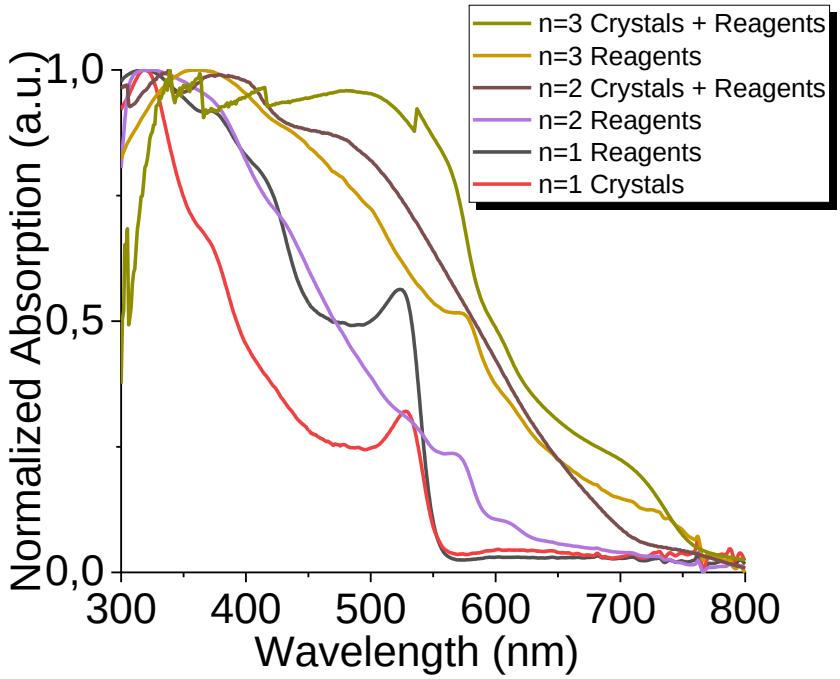

Figure 15. Reflectance spectra of the fabricated n thin film series.

CONCLUSION

The synthesis of the $(Dic)(MA)_{n-1}Pb_nI_{3n+1}$ (n=1-3) thin films proved to be a difficult task. The results for the fabrication of n=1, where the only pure results we obtained, while n=2 and n=3 attempts gave us mixture of phases. Despite the fact that the fabrication of n=2 using stoichiometric ratio of the reagents appeared to be a mixture of phases, traces of n=2 were observed along with n=1 and $MAPbI_3$. On the other hand, the fabrication of n=3 thin films for all batches were the same, as $MAPbI_3$ was making constant appearance.

Chapter 4

OUTLOOK

The synthesis of Bi/Ag and Sb/Ag-based 2D bromide double perovskites and the synthesis of 1D iodide perovskites promotes the success of obtaining double perovskites when the halide is Br^-. Even though the same experiments were conducted in HBr and HI acid, 1D perovskites with Bi and Sb were obtained in HI. Notably, all the new 2D compounds crystallize in the *C 2/c* space group, while all 1D perovskites were crystalized in $P2_12_12_1$ space group. Both 2D double halide perovskites exhibit out of plane tilting along the b axes and the dications have a periodic orientation with the bromide edges looking at the same direction. In contrast, the 1D halide perovskites appear to have the dications facing one another with the iodides being opposite to each other. The energy gap of the 2D halide perovskites is higher than the ones of the 1D perovskites, but still the energy gap of the Bi compounds have slightly lower energy gap than the Sb compounds.

A new homologous series have been synthesized and characterized. The synthesis of $(Dic)(MA)_{n-1}Pb_nI_{3n+1}$ (n = 1-3) homologous series using a new dication with an extra iodine at its structure, promotes a new type of compounds that has the ability to resemble bulk materials. The extra iodine in the formula results in short, I-I distances between the layers, enabling a possible charge transport perpendicular to the perovskite layers. While all perovskites of this series appear to be stable in ambient conditions, n=1 is sensitive and seams to absorb water molecules from the atmosphere, resulting in phase transition. (From red they became yellow) This transition is reversible, when the crystals are under heat they return to their original state. All the compounds are direct narrow bandgap semiconductors with bandgaps between 2.48 eV (n=1) – 1.50 eV ($MPbI_3$). As it was expected, the energy gap increases as the number of layers decreases ($Eg_{hydrated,\ n=1} > Eg_{n=1} > Eg_{n=2} > Eg_{n=3}$). Thin films of the homologous series were synthesized using spin coating method and characterized via XRD and defuse reflectance. Successful was the synthesis of n=1 and in some cases for n=2 as well. For n=3, $MAPbI_3$ was mainly obtained. From the diffuse reflectance measurements appeared that all thin films for n=2 and 3 were mixture of phases. The unpredictable physical properties of the $(Dic)(MA)_{n-1}Pb_nI_{3n+1}$ (n = 1-3) homologous series reported here open new window towards the discovery of new materials of this family so that a better understanding of the electronic properties of these fascinating materials can be achieved.

REFERENCES

1. Hazen, R.M., *Perovskites.* Scientific American, 1988. **258**(6): p. 74-81.
2. Akkerman, Q.A. and L. Manna, *What Defines a Halide Perovskite?* ACS Energy Letters, 2020. **5**(2): p. 604-610.
3. Fu, Y., et al., *Incorporating Large A Cations into Lead Iodide Perovskite Cages: Relaxed Goldschmidt Tolerance Factor and Impact on Exciton–Phonon Interaction.* ACS Central Science, 2019. **5**(8): p. 1377-1386.
4. Wells, H.L., *Über die Cäsium- und Kalium-Bleihalogenide.* Zeitschrift für anorganische Chemie, 1893. **3**(1): p. 195-210.
5. MØLler, C.K., *Crystal Structure and Photoconductivity of Cæsium Plumbohalides.* Nature, 1958. **182**(4647): p. 1436-1436.
6. Auger, V. and T. Karantassis, *Sels complexes de l'iodure stanneux avec les iodures de rubidium et de caesium.* Compt. Rend, 1925. **181**: p. 665-666.
7. Karantassis, T. and L. Capatos, *Sur les complexes iodés du germanium divalent.* Compt. rend, 1935. **201**: p. 74-75.
8. Mao, L., C.C. Stoumpos, and M.G. Kanatzidis, *Two-Dimensional Hybrid Halide Perovskites: Principles and Promises.* Journal of the American Chemical Society, 2019. **141**(3): p. 1171-1190.
9. Kojima, A., et al., *Organometal Halide Perovskites as Visible-Light Sensitizers for Photovoltaic Cells.* Journal of the American Chemical Society, 2009. **131**(17): p. 6050-6051.
10. Ortega-San-Martin, L., *Introduction to Perovskites: A Historical Perspective*, in *Revolution of Perovskite: Synthesis, Properties and Applications*, N.S. Arul and V.D. Nithya, Editors. 2020, Springer Singapore: Singapore. p. 1-41.
11. Ruddlesden, S.N. and P. Popper, *The compound Sr3Ti2O7 and its structure.* Acta Crystallographica, 1958. **11**(1): p. 54-55.
12. Dion, M., M. Ganne, and M. Tournoux, *Nouvelles familles de phases MIMII2Nb3O10 a feuillets "perovskites".* Materials Research Bulletin, 1981. **16**(11): p. 1429-1435.
13. Jacobson, A.J. and J.L. Hutchison, *An investigation of the structure of 12HBaCoO2.6 by electron microscopy and powder neutron diffraction.* Journal of Solid State Chemistry, 1980. **35**(3): p. 334-340.
14. Miller, R.C., *On the origin of Barkhausen pulses in BaTiO3.* Journal of Physics and Chemistry of Solids, 1960. **17**(1): p. 93-100.
15. Liang, R., et al., *Growth and properties of superconducting YBCO single crystals.* Physica C: Superconductivity, 1992. **195**(1): p. 51-58.
16. Wollman, D.A., et al., *Experimental determination of the superconducting pairing state in YBCO from the phase coherence of YBCO-Pb dc SQUIDs.* Physical Review Letters, 1993. **71**(13): p. 2134-2137.
17. Ayache, J. and P.H. Albarède, *Application of the ionless tripod polisher to the preparation of YBCO superconducting multilayer and bulk ceramics thin films.* Ultramicroscopy, 1995. **60**(2): p. 195-206.
18. Katan, C., N. Mercier, and J. Even, *Quantum and Dielectric Confinement Effects in Lower-Dimensional Hybrid Perovskite Semiconductors.* Chemical Reviews, 2019. **119**(5): p. 3140-3192.
19. Cao, D.H., et al., *2D Homologous Perovskites as Light-Absorbing Materials for Solar Cell Applications.* Journal of the American Chemical Society, 2015. **137**(24): p. 7843-7850.
20. Tsai, H., et al., *High-efficiency two-dimensional Ruddlesden-Popper perovskite solar cells.* Nature, 2016. **536**(7616): p. 312-6.

21. Mao, L., et al., *Chemical and Structural Diversity of Hybrid Layered Double Perovskite Halides.* Journal of the American Chemical Society, 2019. **141**(48): p. 19099-19109.
22. Mao, L., et al., *Hybrid Dion–Jacobson 2D Lead Iodide Perovskites.* Journal of the American Chemical Society, 2018. **140**(10): p. 3775-3783.
23. Mao, L., et al., *Seven-Layered 2D Hybrid Lead Iodide Perovskites.* Chem, 2019. **5**(10): p. 2593-2604.
24. Stoumpos, C.C. and M.G. Kanatzidis, *The Renaissance of Halide Perovskites and Their Evolution as Emerging Semiconductors.* Accounts of Chemical Research, 2015. **48**(10): p. 2791-2802.
25. Mercier, N., *Hybrid Halide Perovskites: Discussions on Terminology and Materials.* Angewandte Chemie International Edition, 2019. **58**(50): p. 17912-17917.
26. McClure, E.T., et al., *Cs2AgBiX6 (X = Br, Cl): New Visible Light Absorbing, Lead-Free Halide Perovskite Semiconductors.* Chemistry of Materials, 2016. **28**(5): p. 1348-1354.
27. Volonakis, G., et al., *Cs2InAgCl6: A New Lead-Free Halide Double Perovskite with Direct Band Gap.* The Journal of Physical Chemistry Letters, 2017. **8**(4): p. 772-778.
28. Yusoff, A.R.b.M. and M.K. Nazeeruddin, *Low-Dimensional Perovskites: From Synthesis to Stability in Perovskite Solar Cells.* Advanced Energy Materials, 2018. **8**(26): p. 1702073.
29. Weber, D., *CH3NH3PbX3, ein Pb(II)-System mit kubischer Perowskitstruktur / CH3NH3PbX3, a Pb(II)-System with Cubic Perovskite Structure.* Zeitschrift für Naturforschung B, 1978. **33**(12): p. 1443-1445.
30. Ortiz-Cervantes, C., P. Carmona-Monroy, and D. Solis-Ibarra, *Two-Dimensional Halide Perovskites in Solar Cells: 2D or not 2D?* ChemSusChem, 2019. **12**(8): p. 1560-1575.
31. Kim, H., et al., *2D and Quasi-2D Halide Perovskites: Applications and Progress.* physica status solidi (RRL) – Rapid Research Letters, 2020. **14**(2): p. 1900435.
32. I., D.Y., I. Tamotsu, and M. Yusei, *In Situ X-Ray Observation on the Intercalation of Weak Interaction Molecules into Perovskite-Type Layered Crystals (C9H19NH3)2PbI4 and (C10H21NH3)2CdCl4.* Bulletin of the Chemical Society of Japan, 1986. **59**(2): p. 563-567.
33. Hu, J., L. Yan, and W. You, *Two-Dimensional Organic–Inorganic Hybrid Perovskites: A New Platform for Optoelectronic Applications.* Advanced Materials, 2018. **30**(48): p. 1802041.
34. Lin, C.-W., et al., *Structure-Dependent Photoluminescence in Low-Dimensional Ethylammonium, Propylammonium, and Butylammonium Lead Iodide Perovskites.* ACS Applied Materials & Interfaces, 2020. **12**(4): p. 5008-5016.
35. Vashishtha, P., et al., *High Efficiency Blue and Green Light-Emitting Diodes Using Ruddlesden–Popper Inorganic Mixed Halide Perovskites with Butylammonium Interlayers.* Chemistry of Materials, 2019. **31**(1): p. 83-89.
36. Wang, Z., et al., *Spacer Cation Tuning Enables Vertically Oriented and Graded Quasi-2D Perovskites for Efficient Solar Cells.* Advanced Functional Materials, 2021. **31**(5): p. 2008404.
37. Stoumpos, C.C., et al., *Structure–Band Gap Relationships in Hexagonal Polytypes and Low-Dimensional Structures of Hybrid Tin Iodide Perovskites.* Inorganic Chemistry, 2017. **56**(1): p. 56-73.
38. Slavney, A.H., et al., *A Bismuth-Halide Double Perovskite with Long Carrier Recombination Lifetime for Photovoltaic Applications.* Journal of the American Chemical Society, 2016. **138**(7): p. 2138-2141.
39. Slavney, A.H., et al., *Defect-Induced Band-Edge Reconstruction of a Bismuth-Halide Double Perovskite for Visible-Light Absorption.* Journal of the American Chemical Society, 2017. **139**(14): p. 5015-5018.

40. Jana, M.K., et al., *Direct-Bandgap 2D Silver–Bismuth Iodide Double Perovskite: The Structure-Directing Influence of an Oligothiophene Spacer Cation.* Journal of the American Chemical Society, 2019. **141**(19): p. 7955-7964.
41. Menedjhi, A., et al., *Halide double perovskite Cs2AgInBr6 for photovoltaic's applications: Optical properties and stability.* Optik, 2021. **243**: p. 167198.
42. Li, X., et al., *Bismuth/Silver-Based Two-Dimensional Iodide Double and One-Dimensional Bi Perovskites: Interplay between Structural and Electronic Dimensions.* Chemistry of Materials, 2021. **33**(15): p. 6206-6216.
43. Volonakis, G., et al., *Lead-Free Halide Double Perovskites via Heterovalent Substitution of Noble Metals.* The Journal of Physical Chemistry Letters, 2016. **7**(7): p. 1254-1259.
44. Ramalingam, K., et al., *Synthesis of nitroimidazole substituted 3,3,9,9-tetramethyl-4,8-diazaundecane-2,10-dione dioximes (propylene amine oximes, PnAOs): Ligands for technetium-99m complexes with potential for imaging hypoxic tissue.* Tetrahedron, 1995. **51**(10): p. 2875-2894.
45. Christy, A.A., O.M. Kvalheim, and R.A. Velapoldi, *Quantitative analysis in diffuse reflectance spectrometry: A modified Kubelka-Munk equation.* Vibrational Spectroscopy, 1995. **9**(1): p. 19-27.
46. Momma, K. and F. Izumi, *VESTA: a three-dimensional visualization system for electronic and structural analysis.* Journal of Applied Crystallography, 2008. **41**(3): p. 653-658.
47. Chondroudis, K., T.J. McCarthy, and M.G. Kanatzidis, *Chemistry in Molten Alkali Metal Polyselenophosphate Fluxes. Influence of Flux Composition on Dimensionality. Layers and Chains in APbPSe4, A4Pb(PSe4)2 (A = Rb, Cs), and K4Eu(PSe4)2.* Inorganic Chemistry, 1996. **35**(4): p. 840-844.
48. McCarthy, T.J. and M.G. Kanatzidis, *Synthesis in Molten Alkali Metal Polyselenophosphate Fluxes: A New Family of Transition Metal Selenophosphate Compounds, A2MP2Se6 (A = K, Rb, Cs; M = Mn, Fe) and A2M'2P2Se6 (A = K, Cs; M' = Cu, Ag).* Inorganic Chemistry, 1995. **34**(5): p. 1257-1267.
49. Vasileiadou, E.S., et al., *Insight on the Stability of Thick Layers in 2D Ruddlesden–Popper and Dion–Jacobson Lead Iodide Perovskites.* Journal of the American Chemical Society, 2021. **143**(6): p. 2523-2536.
50. Leblanc, A., et al., *Lead- and Iodide-Deficient (CH3NH3)PbI3 (d-MAPI): The Bridge between 2D and 3D Hybrid Perovskites.* Angewandte Chemie International Edition, 2017. **56**(50): p. 16067-16072.
51. Dahlman, C.J., et al., *Structural Evolution of Layered Hybrid Lead Iodide Perovskites in Colloidal Dispersions.* ACS Nano, 2020. **14**(9): p. 11294-11308.
52. Ke, W., et al., *Narrow-Bandgap Mixed Lead/Tin-Based 2D Dion–Jacobson Perovskites Boost the Performance of Solar Cells.* Journal of the American Chemical Society, 2020. **142**(35): p. 15049-15057.
53. Stoumpos, C.C., et al., *Ruddlesden–Popper Hybrid Lead Iodide Perovskite 2D Homologous Semiconductors.* Chemistry of Materials, 2016. **28**(8): p. 2852-2867.
54. Zhu, X.-H., et al., *(C4H3SCH2NH3)2(CH3NH3)Pb2I7 : non-centrosymmetrical crystal structure of a bilayer hybrid perovskite.* Chemical Communications, 2002(18): p. 2160-2161.
55. Li, Y., et al., *Synthesis, structure and optical properties of different dimensional organic–inorganic perovskites.* Solid State Sciences, 2007. **9**(9): p. 855-861.
56. Gao, L., et al., *m-Phenylenediammonium as a New Spacer for Dion–Jacobson Two-Dimensional Perovskites.* Journal of the American Chemical Society, 2021. **143**(31): p. 12063-12073.

57. Xiong, K., et al., *New hybrid lead iodides: From one-dimensional chain to two-dimensional layered perovskite structure.* Journal of Solid State Chemistry, 2015. **230**: p. 143-148.
58. Lemmerer, A. and D.G. Billing, *Lead halide inorganic–organic hybrids incorporating diammonium cations.* CrystEngComm, 2012. **14**(6): p. 1954-1966.
59. Momma, K. and F. Izumi, *VESTA 3 for three-dimensional visualization of crystal, volumetric and morphology data.* Journal of Applied Crystallography, 2011. **44**(6): p. 1272-1276.
60. Andrews, D.L., *Quantum dynamics of simple systems.* Quantum and Semiclassical Optics: Journal of the European Optical Society Part B, 1996. **8**(6): p. 010.
61. Shi, E., et al., *Extrinsic and Dynamic Edge States of Two-Dimensional Lead Halide Perovskites.* ACS Nano, 2019. **13**(2): p. 1635-1644.
62. Miao, Y., et al., *Designable Layer Edge States in Quasi-2D Perovskites Induced by Femtosecond Pulse Laser.* Advanced Science, 2022. **9**(20): p. 2201046.
63. Blancon, J.-C., et al., *Extremely efficient internal exciton dissociation through edge states in layered 2D perovskites.* Science, 2017. **355**(6331): p. 1288-1292.
64. Stoumpos, C.C., et al., *High Members of the 2D Ruddlesden-Popper Halide Perovskites: Synthesis, Optical Properties, and Solar Cells of (CH3(CH2)3NH3)2(CH3NH3)4Pb5I16.* Chem, 2017. **2**(3): p. 427-440.
65. Kim, H.-S., et al., *Lead Iodide Perovskite Sensitized All-Solid-State Submicron Thin Film Mesoscopic Solar Cell with Efficiency Exceeding 9%.* Scientific Reports, 2012. **2**(1): p. 591.
66. Lee, M.M., et al., *Efficient hybrid solar cells based on meso-superstructured organometal halide perovskites.* Science, 2012. **338**(6107): p. 643-7.
67. Burschka, J., et al., *Sequential deposition as a route to high-performance perovskite-sensitized solar cells.* Nature, 2013. **499**(7458): p. 316-319.
68. Jeon, N.J., et al., *Solvent engineering for high-performance inorganic-organic hybrid perovskite solar cells.* Nat Mater, 2014. **13**(9): p. 897-903.
69. Zhou, H., et al., *Photovoltaics. Interface engineering of highly efficient perovskite solar cells.* Science, 2014. **345**(6196): p. 542-6.
70. Jung, H.S. and N.-G. Park, *Perovskite Solar Cells: From Materials to Devices.* Small, 2015. **11**(1): p. 10-25.
71. Park, J., et al., *Controlled growth of perovskite layers with volatile alkylammonium chlorides.* Nature, 2023. **616**(7958): p. 724-730.
72. Mitzi, D.B., *Synthesis, Structure, and Properties of Organic-Inorganic Perovskites and Related Materials*, in *Progress in Inorganic Chemistry*. 1999. p. 1-121.
73. Baikie, T., et al., *Synthesis and crystal chemistry of the hybrid perovskite (CH3NH3)PbI3 for solid-state sensitised solar cell applications.* Journal of Materials Chemistry A, 2013. **1**(18): p. 5628-5641.
74. D'Innocenzo, V., et al., *Excitons versus free charges in organo-lead tri-halide perovskites.* Nature Communications, 2014. **5**(1): p. 3586.

APPENDIX SCHEME

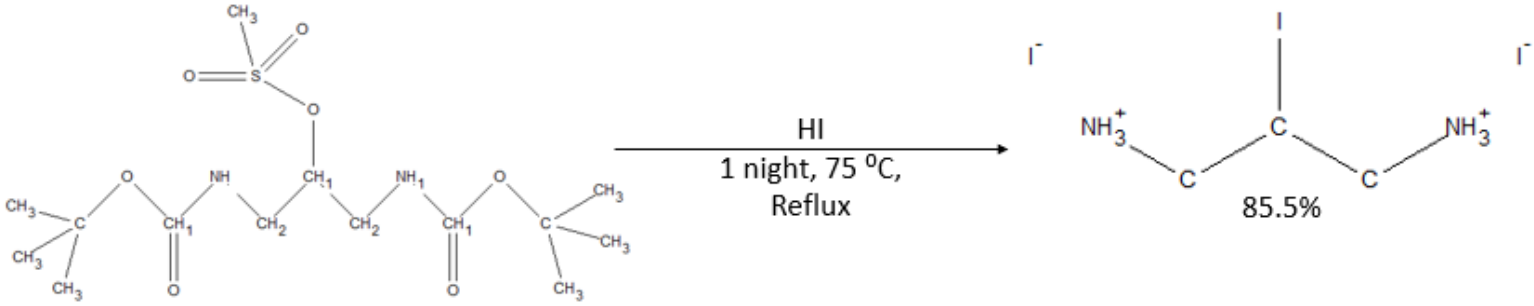

Scheme S1. Synthetical process of the DicI,I_2 salt from the commercial 1,3- aminopropan-2-ol molecule.

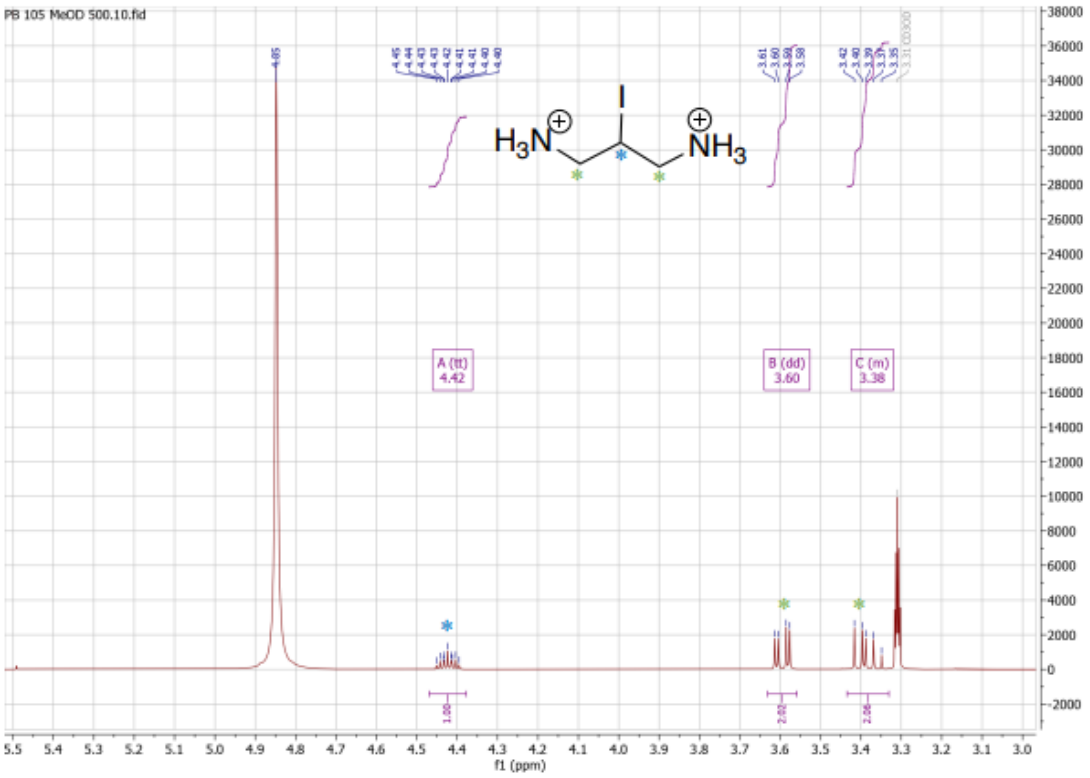

Scheme S2. Proton NMR of 2-iodopropan-1,3-diamonium diiodide salt in deuterated methanol

^{1}H NMR (499 MHz, Methanol-d4) δ 4.42 (tt, J = 9.7, 4.3 Hz, 1H), 3.60 (dd, J = 14.1, 4.3 Hz, 2H), 3.43 – 3.33 (m, 2H)

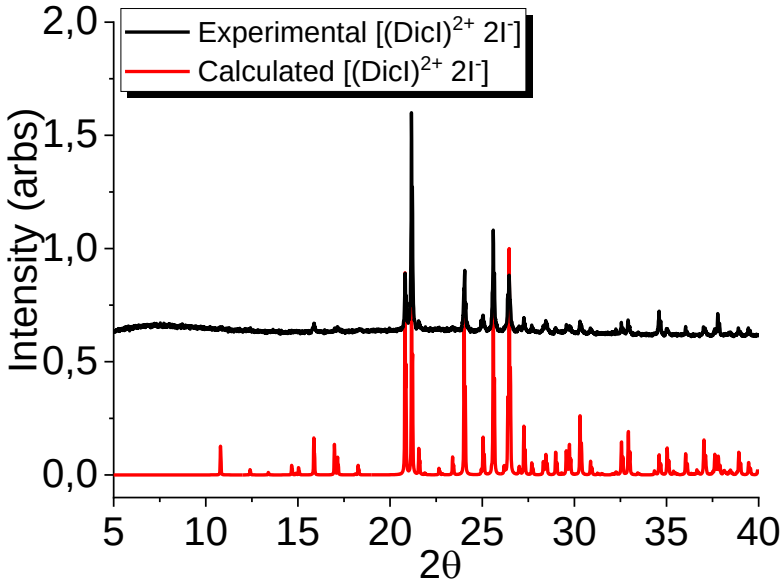

Scheme S3. XRD pattern of 2-iodopropan-1,3-diamonium diiodide salt.

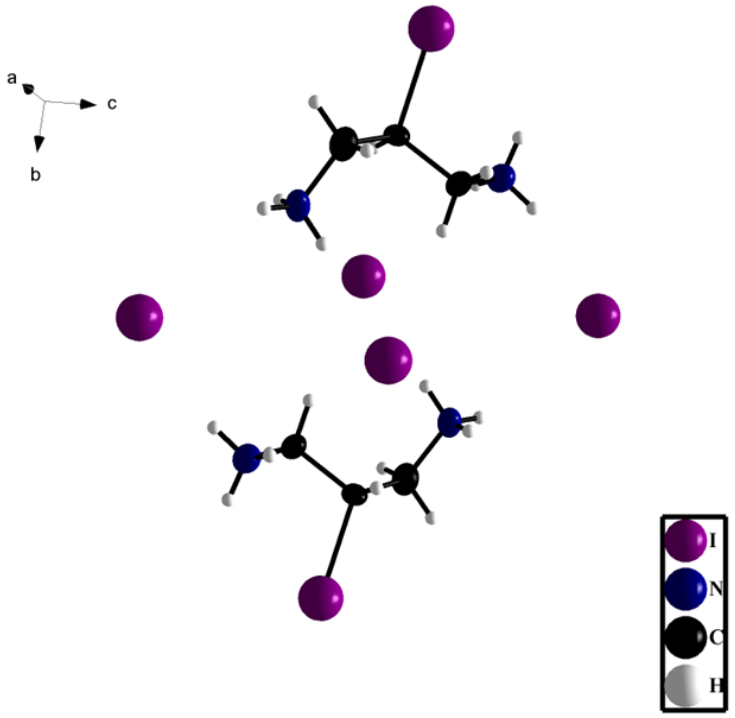

Scheme S4. Illustration of the 2-iodopropan-1,3-diamonium diiodide salt.

Schematic Table 1. Crystallographic Data for the 2-iodopropan-1,3-diamonium diiodide salt. at 293K.

2-iodopropane-1,3-diamonium diiodide [$(DicI)^{2+}$ $2I^-$]	
Empirical Formula	$C_3 H_{11} N_2 I_3$
Crystal System	monoclinic
Space Group	P 1 21/n 1
Unit Cell Dimensions	
a (Å)	a = 7.5743
b (Å)	b = 10.4359
c(Å)	c = 13.5187
α (deg)	α = 90
β (deg)	β = 102.1722
γ (deg)	γ = 90
Volume ($Å^3$)	1044.557
Z	4
Density (gr/cm^3)	2.8987
Independent Reflections	1892 [Rint = 0.1162]
Data/restrains/parameters	1892 / 0 / 73
Final *R* Indices [I>2σ(I)]	Robs = 0.0441, wRobs = 0.0493
R indices [all data]	Rall = 0.0571, wRall = 0.0500
Fourier Difference max and min ($e \cdot Å^{-3}$)	4.89 and -3.34

Appendix

Table S1. Crystallographic Data for the 2D and 1D compounds at 293K.

Compound	$(DicBr)_2AgBiBr_9$	$(DicBr)_2AgSbBr_9$	$(DicI)BiI_5$	$(DicI)SbI_5$
Empirical Formula	$(C_6 N_4 H_{14})$ Ag Bi Br_9	$(C_6 N_4 H_{14})$ Ag Sb Br_9	$(C_3 H_{11} N_2 I_1)$ Bi I_5	$(C_3 H_{11} N_2 I_1)$ Sb I_5
Formula Weight	1178.2	1178.9	958.1	958.3
Temperature (K)	282 K	293	287	287
Wavelength (Å)	1.54187 Å	0.71073	1.54184	1.54184
Crystal System	monoclinic	monoclinic	orthorhombic	orthorhombic
Space Group	C 1 2/c 1	C 1 2/c 1	P 2_1 2_1 2_1	P 2_1 2_1 2_1
Unit Cell Dimens **a (Å)** **b (Å)** **c(Å)** **α (deg)** **β (deg)** **γ (deg)**	a = 18.4240(13) b = 11.8574(8) c = 11.5770(8) α = 90 β = 90.524(6) γ = 90	a = 18.4352(10) b = 11.8743(7) c = 11.5577(8) α = 90(5) β = 90.046(5) γ = 90(5)	a = 8.4626(5) b = 13.2998(7) c = 14.8776(6) α = 90 β = 90 γ = 90	a = 8.4626(5) b = 13.2998(7) c = 14.8776(6) α = 90 β = 90 γ = 90
V ($Å^3$)	2529.0(3)	2530.0(3)	1674.49(15)	1674.49(15)
Z	4	4	4	4
Density (g/cm^3)	3.0944	3.0951	3.8013	3.8013
Absorption Coefficient (mm^{-1})	36.368	17.635	99.69	99.69
F(000)	2264	2136	1648	1648
Crystal Size (mm^3)	? x ? x ?	? x ? x ?	? x ? x ?	? x ? x ?
θ Range for Data Collection (deg)	4.43 to 76.47	2.04 to 40.92	4.46 to 76.46	4.46 to 76.46
Index Ranges	$-18 \leq h \leq 23$ $-14 \leq k \leq 14$ $-14 \leq l \leq 14$	$-29 \leq h \leq 32$ $-17 \leq k \leq 20$ $-18 \leq l \leq 18$	$-7 \leq h \leq 12$ $-14 \leq k \leq 14$ $-9 \leq l \leq 18$	$-9 \leq h \leq 10$ $-16 \leq k \leq 16$ $-13 \leq l \leq 18$
Reflections Collected	6212	86017	8266	8266
Independent Reflections	2273 [R_{int} = 0.078]	2290 [R_{int} = 0.1532]	3016 [R_{int} = 0.0901]	3016 [R_{int} = 0.0901]
Completeness to θ = 35.04° (%)	98	98	99	99
Refinement Method	Full-matrix least squares on F^2.			
Data / Restraints / Parameters	2273 / 0 / 103	2290 / 0 / 78	3016 / 0 / 85	3016 / 0 / 85
Goodness-of-Fit	4.43	9.28	1.49	1.49
Final R Indices [I>2σ(I)]	R_{obs} = 0.1515, wR_{obs} = 0.1465	R_{obs} = 0.1983 wR_{obs} = 0.2588	R_{obs} = 0.0615 wR_{obs} = 0.0695	R_{obs} = 0.0615 wR_{obs} = 0.0695

R Indices [all data]	R_{all} = 0.1550, wR_{all} = 0.1468	R_{all} = 0.2025 wR_{all} = 0.2590	R_{all} = 0.0664 wR_{all} = 0.0703	R_{all} = 0.0664 wR_{all} = 0.0703
Fourier Difference max and min ($e \cdot Å^{-3}$)	8.22 and -1.93	5.60 and -9.45	2.25 and -2.04	2.25 and -2.04

Table 2. Bond Distances for the 2D and 1D compounds

$(DicBr)_2AgBiBr_9$		**$(DicBr)_2AgSbBr_9$**		**$(DicI)BiI_5$**		**$(DicI)SbI_5$**	
Label	Distances (Å)	Label	Distances (Å)	Label	Distances (Å)	Label	Distances (Å)
Bi(1)-Br(2)	2.839(3)	Sb(1)-Br(2)	2.771(7)	Bi(1)-I(1)	2.8762(18)	Sb(1)-I(1)	2.8762(18)
Bi(1)-Br(4)	2.865(3)	Sb(1)-Br(3)	2.873(9)	Bi(1)-I(2)	2.8667(18)	Sb(1)-I(2)	2.8667(18)
Bi(1)-Br(5)	2.872(4)	Sb(1)-Br(6)	2.897(9)	Bi(1)-I(3)	2.986(2)	Sb(1)-I(3)	2.986(2)
Bi(1)-Br(6)	2.828(4)	Sb(1)-Br(4)	2.923(7)	Bi(1)-I(4)	3.061(2)	Sb(1)-I(4)	3.061(2)
Average	2.851.		2.866	Bi(1)-I(6)	3.169(2)	Sb(1)-I(6)	3.169(2)
Ag(1)-Br(6)	3.110(6)	Ag(1)-Br(1)	2.670(7)				
Ag(1)-Br(3)	2.586(3)	Ag(1)-Br(3)	3.077(10)				
Ag(1)-Br(5)	3.047(5)	Ag(1)-Br(6)	3.026(11)				
Ag(1)-Br(4)	3.183(3)	Ag(1)-Br(4)	3.101(7)				
Average	2.982		2.969		2.9916		2.9918
Br(1)-C(1)	1.93(3)	Br(5)-C(3)	1.84(6)	I(5)-C(1)	2.17(2)	I(5)-C(1)	2.17(2)

Table S3. Bond Angles for the 2D and 1D Compounds Reported Here

$(DicBr)_2AgBiBr_9$		**$(DicBr)_2AgSbBr_9$**		**$(DicI)BiI_5$**		**$(DicI)SbI_5$**	
Label	Angle (°)	Label	Angle (°) In plane	Label	Angle (°) In plane	Label	Angle (°) In plane
Bi(1)-Br(4)-Ag(1)	147.60(11)	Sb(1)-Br(4)-Ag(1)	148.6(3)	Sb(1)-I(6)-Sb(1)	159.10(7)	Sb(1)-I(6)-Sb(1)	160.10(7)
Bi(1)-Br(5)-Ag(1)	180.00(0)	Sb(1)-Br(3)-Ag(1)	180.00(0)				
Average	168.80		164.30		159.10(7)		160.10(7)

Table S4. Crystallographic Data for (Dic)$(MA)_{n-1}Pb_nI_{3n+1}$ at 293K.

Compound	(DicI)$PbI_4 \cdot 1H_2O$	(DicI)PbI_4	(DicI)(MA)Pb_2I_7	(DicI)$(MA)_2Pb_3I_{10}$
Empirical Formula	$(C_3\ N_2\ H_{13}\ I_1\ O_1)\ Pb_1\ I_4$	$(C_3\ N_2\ H_{11}\ I_1)\ Pb_1\ I_4$	$(C_3\ H_{11}\ N_2\ I_1)\ (C_1\ N_1\ H_6)$ $Pb_2\ I_7$	$(C_3\ H_{11}\ N_2\ I_1)\ (C_1\ N_1\ H_6)_2\ Pb_3$ I_{10}
Formula Weight	934.9	916.8	1536.8	2156.8
Temperature (K)	293.6	293	293	293
Wavelength (Å)	1.54184	1.54184	1.54184	1.54184
Crystal System	monoclinic	orthorhombic	orthorhombic	orthorhombic
Space Group	P 1 21/c 1	C m c e	P b a m	A e a 2
Unit Cell Dimens **a (Å)** **b (Å)** **c(Å)** **α (deg)** **β (deg)** **γ (deg)**	a = 6.5423 b = 14.9998 c = 16.7321 α = 90 β = 94.941 γ = 90	a = 20.1168(15) b = 12.6758(10) c = 12.2263(7) α = 90 β = 90 γ = 90	a = 12.3289(8) b = 12.7636(7) c = 16.2040(9) α = 90 β = 90 γ = 90	a = 12.3926(5) b = 12.7378(5) c = 44.8986(15) α = 90 β = 90 γ = 90
V (Å^3)	1635.873	3117.7(4)	2793.813	7087.4(5)
Z	4	8	4	8
Density (g/cm^3)	3.7958	3.9067	4.0032	4.0426
Absorption Coefficient (mm^{-1})	93.951	98.516	101.352	102.52
F(000)	1600	3120	2600	7280
Crystal Size (mm^3)	0.186 x 0.142 x 0.046	? x ? x ?	? x ? x ?	? x ? x ?
θ Range for Data Collection (deg)	3.96 to 75.96	4.4 to 67.67	2.73 to 67.68	3.94 to 67.68
Index Ranges	-7<=h<=7, -18<=k<=18, -20<=l<=20	$0 \le h \le 24$ $0 \le k \le 15$ $0 \le l \le 14$	$0 \le h \le 14$ $0 \le k \le 15$ $0 \le l \le 19$	$0 \le h \le 14$ $0 \le k \le 15$ $-53 \le l \le 53$
Reflections Collected	6895	1462	2398	6181
Independent Reflections	2954 [R_{int} = 0.1612]	1462 [R_{int} = N/A]	2398 [R_{int} = N/A]	6181 [R_{int} = N/A]
Completeness to θ = 35.04° (%)	98	100	100	100
Refinement Method	Full-matrix least squares on F^2.			
Data / Restraints / Parameters	2954 / 0 / 109	1462 / 0 / 66	2398 / 0 / 86	6181 / 9 / 176
Goodness-of-Fit	2.34	1.55	1.08	1.71
Final R Indices [I>2σ(I)]	R_{obs} = 0.1328, wR_{obs} = 0.1373	R_{obs} = 0.0473 wR_{obs} = 0.0519	R_{obs} = 0.0311 wR_{obs} = 0.0329	R_{obs} = 0.0533 wR_{obs} = 0.1129
R Indices [all data]	R_{all} = 0.1546,	R_{all} = 0.0652	R_{all} = 0.0451	R_{all} = 0.0668

	wR_{all} = 0.1425	wR_{all} = 0.0546	wR_{all} = 0.0349	wR_{all} = 0.1180
Fourier Difference max and min ($e \cdot Å^{-3}$)	8.94 and -7.26	5.39 and -1.85	4.77 and -1.24	4.78 and -1.72

Table S5. Bond Distances for $(Dic)(MA)_{n-1}Pb_nI_{3n+1}$

$(DicI)PbI_4 \cdot 1H_2O$		**$(DicI)PbI_4$**		**$(DicI)(MA)Pb_2I_7$**		**$(DicI)(MA)_2Pb_3I_{10}$**	
Label	Distances (Å)	Label	Distances (Å)	Label	Distances (Å)	Label	Distances (Å)
Pb(1)-I(2)	3.124(3)	Pb(1)-I(1)	3.2250(7)	Pb(1)-I(1)	3.0696(8)	Pb(1)- I(1)	3.182(2)
Pb(1)-I(3)	3.284(3)	Pb(1)-I(2)	3.1529(11)	Pb(1)-I(2)	3.2310(6)	Pb(1)-I(5)	3.039(4)
Pb(1)-I(3)	3.301(2)	Pb(1)-I(3)	3.1736(18)	Pb(1)-I(3)	3.1902(8)	Pb(1)-I(7)	3.337(4)
Pb(1)-I(4)	3.107(2)			Pb(1)-I(4)	3.1897(6)	Pb(1)-I(13)	3.242(2)
Pb(1)-I(5)	3.240(4)			Pb(1)-I(5)	3.2733(5)	Pb(1)-I(8)	3.174(4)
Pb(1)-I(5)	3.305(35)					Pb(1)-I(8)	3.196(4)
						Pb(2)- I(3)	3.154(3)
						Pb(2)-I(4)	3.200(5)
						Pb(2)-I(7)	3.150(5)
						Pb(2)-I(10)	3.1764(13)
						Pb(2)-I(10)	3.1929(13)
						Pb(2)-I(12)	3.177(3)
						Pb(3)- I(2)	3.243(3)
						Pb(3)-I(4)	3.269(4)
						Pb(3)-I(6)	3.069(4)
						Pb(3)-I(11)	3.187(4)
						Pb(3)-I(11)	3.182(2)
						Pb(3)-I(14)	3.184(2)
Average	3.2268		3.1838		3.1908		3.1863
I(1)-C(3)	2.18(5)	I(4)-C(2)	2.17(2)	I(6)-C(2)	2.150(13)	I(9)-C(3)	2.220(15)

Table S6. Bond Angles for (Dic)$(MA)_{n-2}Pb_nI_{3n+1}$ Compounds Reported Here

(DicI)$PbI_4 \cdot 1H_2O$		**(DicI)PbI_4**		**(DicI)(MA)Pb_2I_7**		**(DicI)$(MA)_2Pb_3I_{10}$**	
Label	Angle (°)	Label	Angle (°) In plane	Label	Angle (°) In plane	Label	Angle (°) In plane
Pb(1)-I(5)-Pb(1)	177.15(119)			Pb(1)-I(3)-Pb(1)	178.74(25)	Pb(1)-I(8)-Pb(1)	178.48
Pb(1)-I(3)-Pb(1)	95.63(65)					Pb(2)-I(10)-Pb(2)	178.73
						Pb(3)-I(11)-Pb(3)	179.63
		Average	180		178.74(25)		178.95
		Label	Angle (°) Out of plane	Label	Angle (°) Out of plane	Label	Angle (°) Out of plane
		Pb(1)-I(3)-Pb(1)	180	Pb(1)-I(4)-Pb(1)	149.75(10)	Pb(1)-I(7)-Pb(2)	158.49
		Pb(1)-I(1)-Pb(1)	143.47(7)	Pb(1)-I(2)-Pb(1)	146.50(10)	Pb(2)-I(4)-Pb(3)	158.93
				Pb(1)-I(5)-Pb(1)	158.20(10)	Pb(3)-I(14)-Pb(3)	150.75
						Pb(3)-I(2)-Pb(3)	148.36
						Pb(2)-I(3)-Pb(2)	157.61
						Pb(2)-I(12)-Pb(2)	155.29
						Pb(1)-I(3)-Pb(1)	148.95
						Pb(1)-I(1)-Pb(1)	150.61
Average	136.39		161.47		151.48		153.62

APPENDIX FIGURES

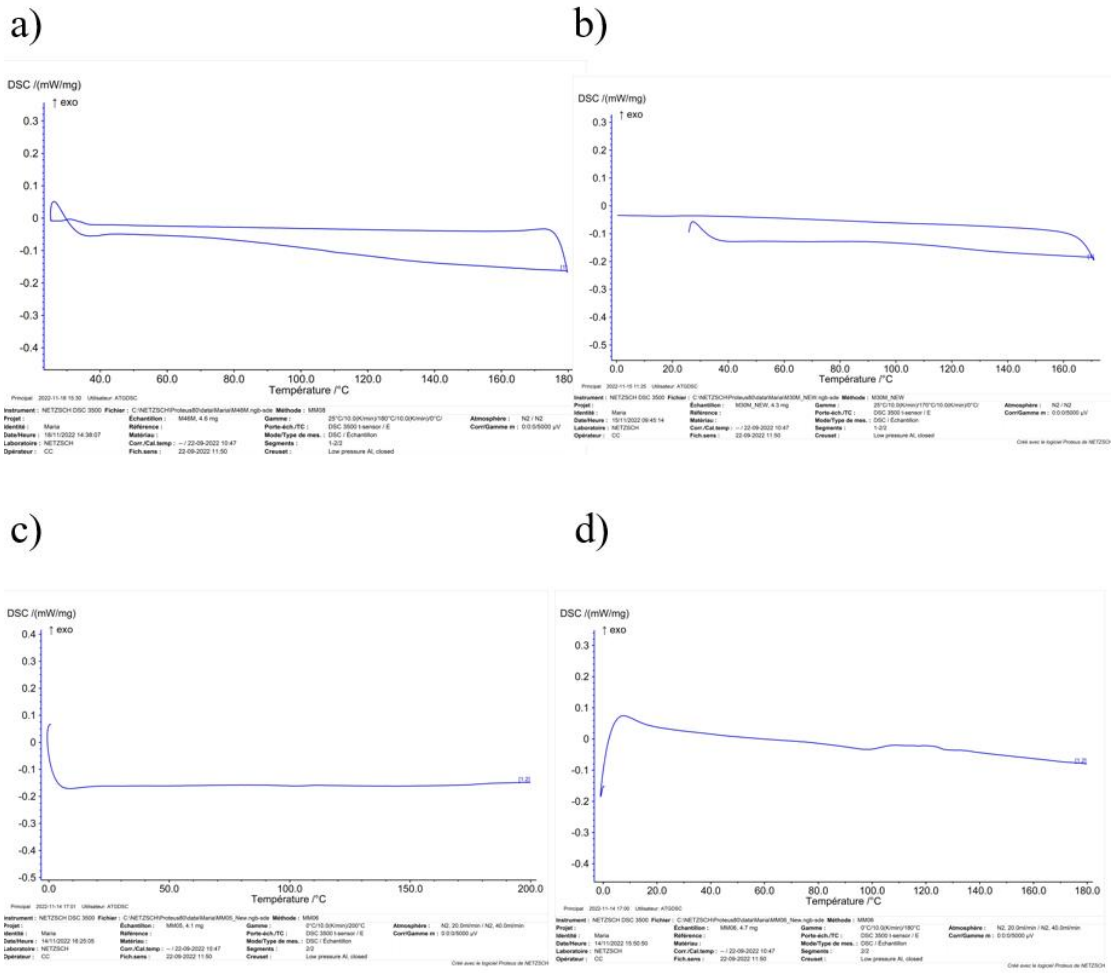

Figure S1. DSC analysis of the 2D double halide perovskites a) $(DicBr)_2AgBiBr_9$ b) $(DicBr)_2AgSbBr_9$ and of the 1D c) $(DicI)BiI_5$ and d) $(DicI)SbI_5$ perovskites.

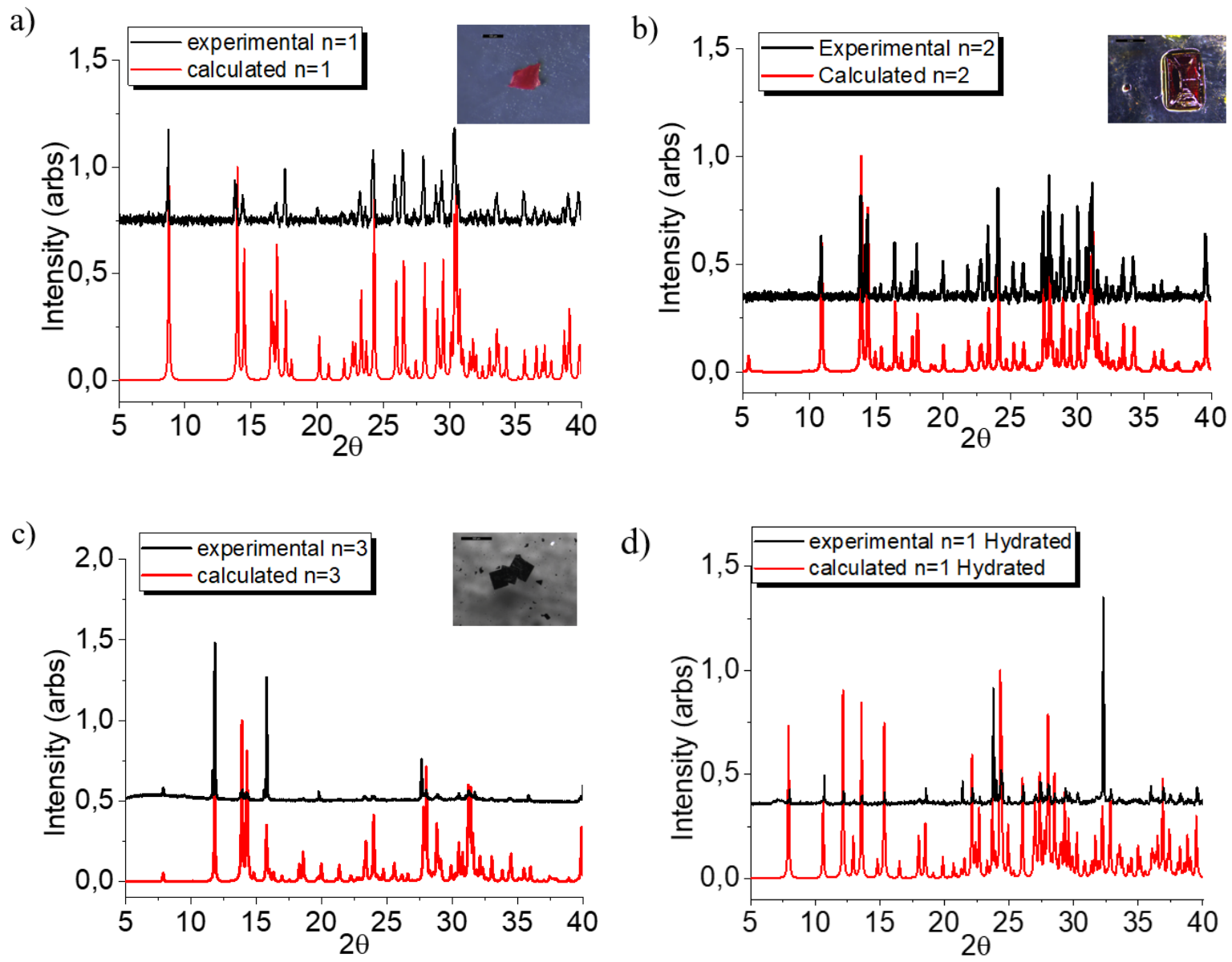

Figure S2. Powder X-ray diffraction (PXRD) patterns of the experimental a) n=1 b) n=2, c) n=3 and d) n=1 hydrated compounds compared to their calculated patterns.

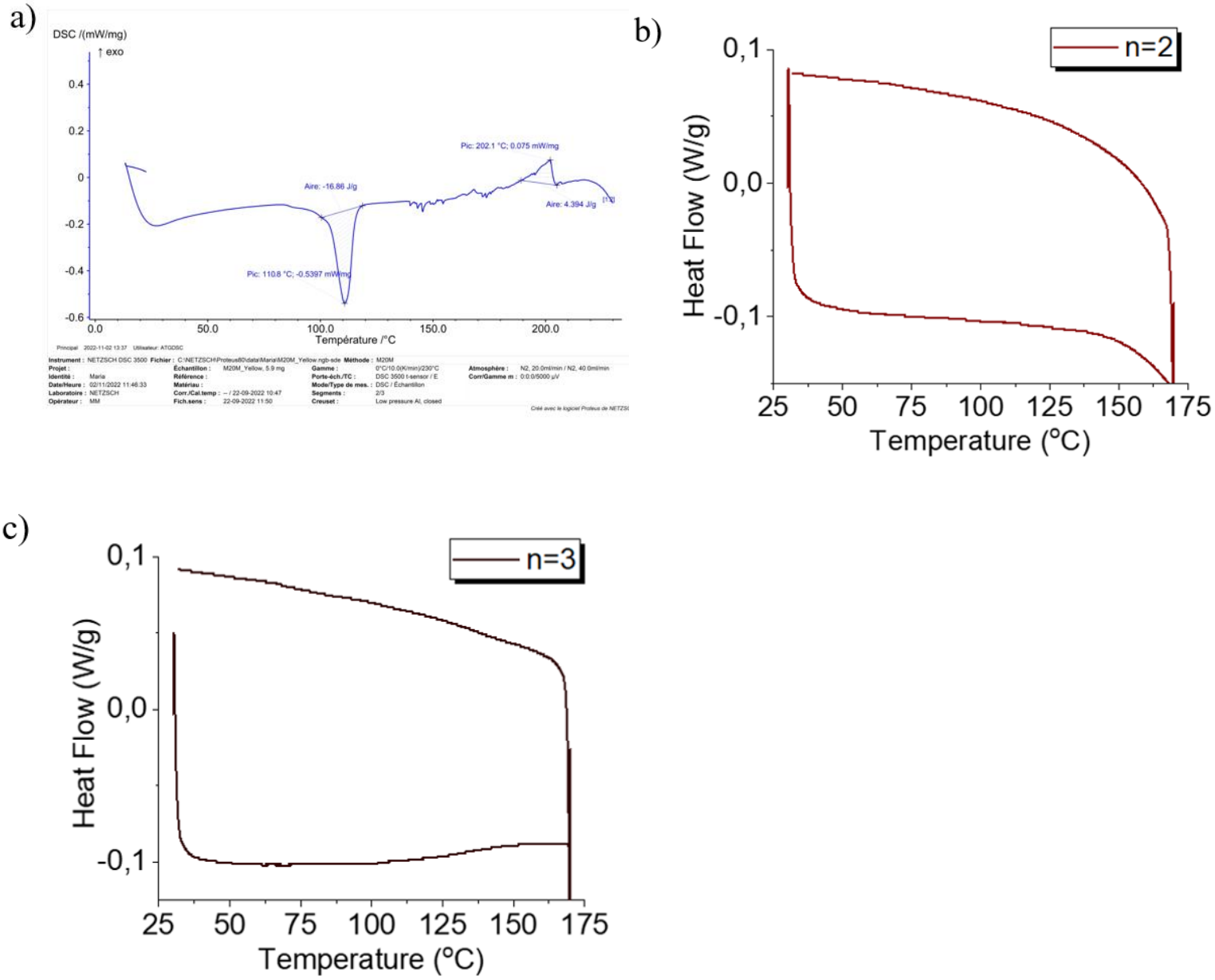

Figure S3. Differential Scanning Calorimetry (DSC) diagrams (a-c) of the n=1hydrated, 2 and 3 compounds.

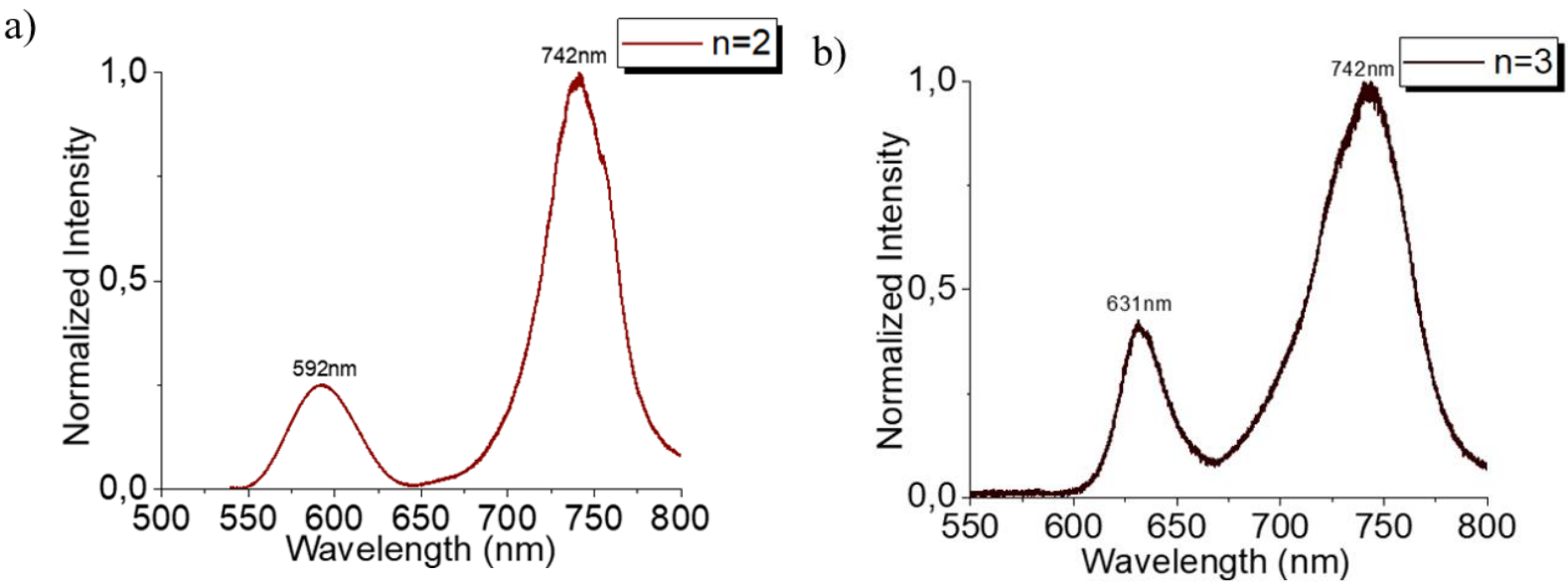

Figure S4. Photoluminescent spectra (PL) for the n compounds, a) n=2, with the main peak at 592nm and the edge effect appearing at 742nm and b) n=3, with the main peak at 631nm and the edge effect appearing at 742nm, with 742nm corresponding to the photoluminescence of the bulk material[61, 63].

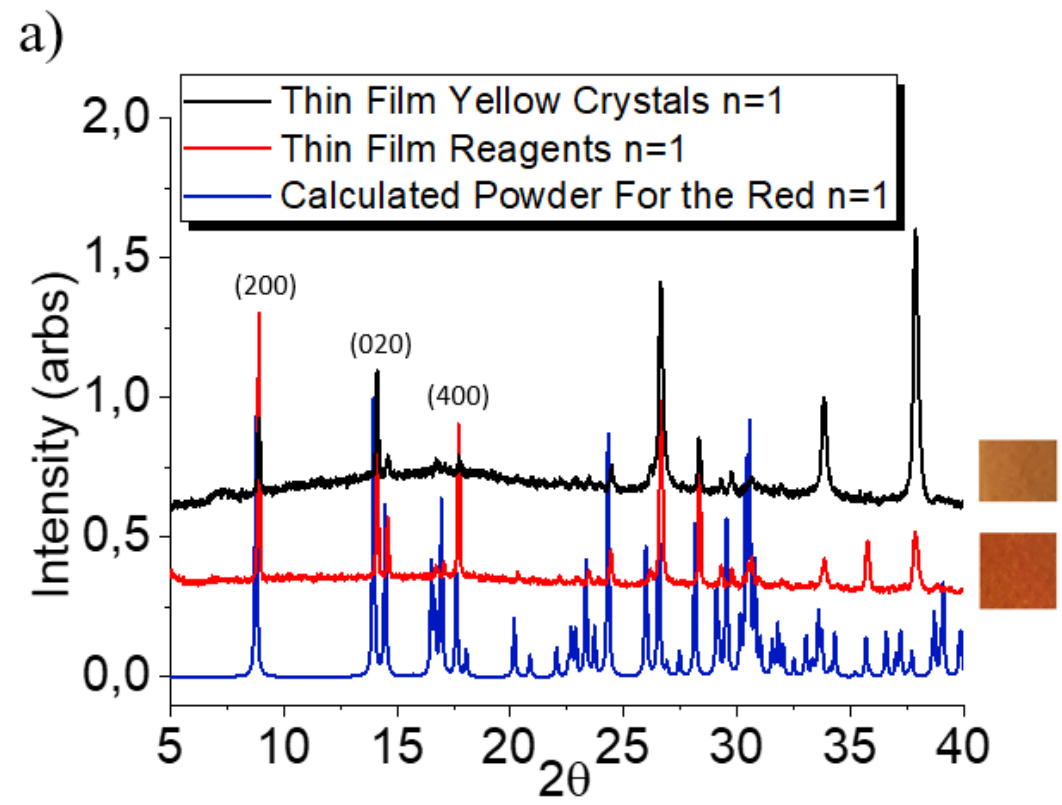
a)
Thin Film Yellow Crystals n=1
Thin Film Reagents n=1
Calculated Powder For the Red n=1
(200)
(020)
(400)
Intensity (arbs)
2θ

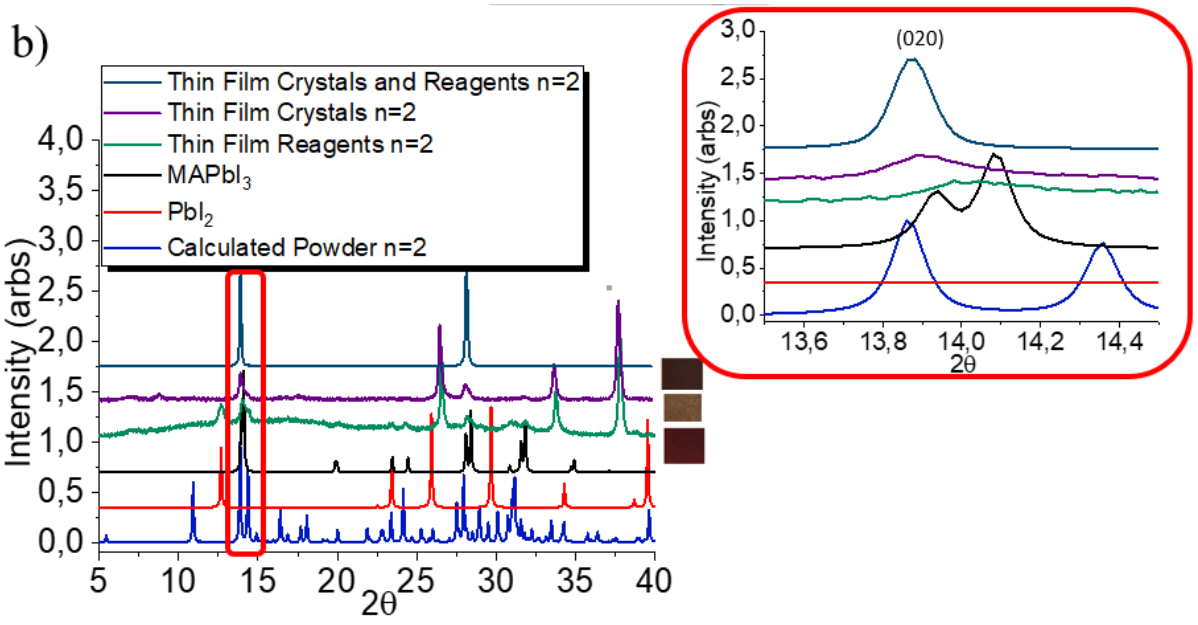
b)
Thin Film Crystals and Reagents n=2
Thin Film Crystals n=2
Thin Film Reagents n=2
MAPbI3
PbI2
Calculated Powder n=2
Intensity (arbs)
2θ
(020)

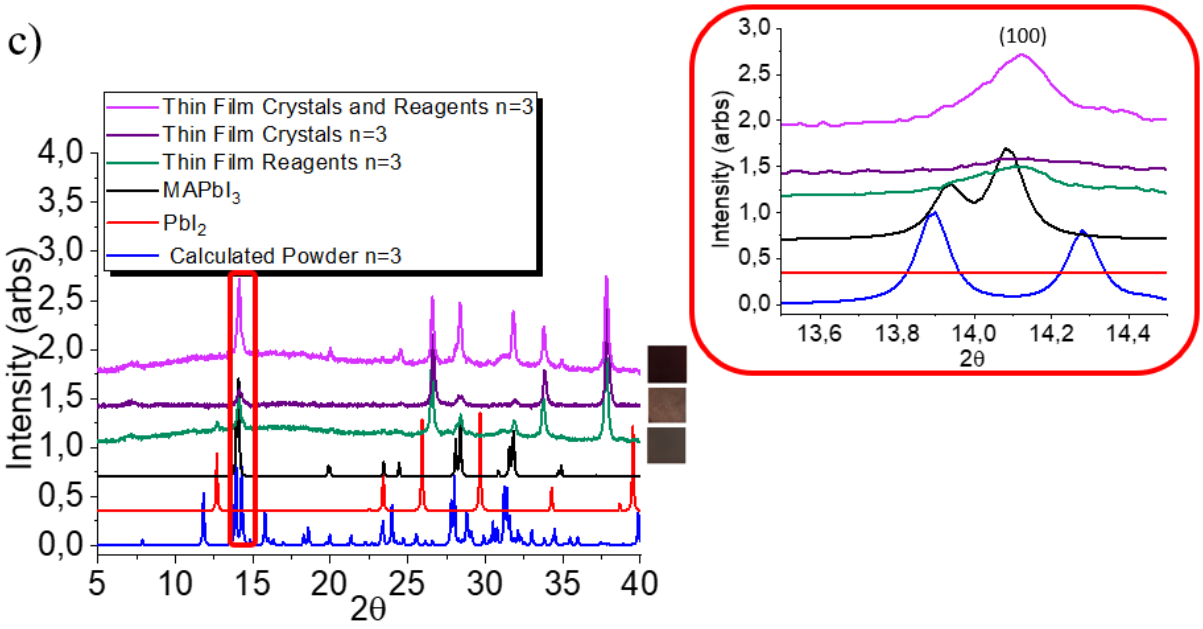

Figure S5. All the Powder X-ray diffraction (PXRD) patterns of a) n=1 thin film attempts, b) n=2 and c) n=3 thin films comparing them with $MAPbI_3$ and PbI_2.